

High frequency isolated bidirectional dual active bridge DC-DC converters and its application to distributed energy systems: an overview

Kiran Bathala, Dharavath Kishan, Nagendrappa Harischandrappa

Department of Electrical and Electronics Engineering, National Institute of Technology Karnataka, Surathkal, India

Article Info

Article history:

Received Nov 1, 2022

Revised Jan 19, 2023

Accepted Feb 1, 2023

Keywords:

Dual active bridge

Energy storage system

Isolated converters

Phase shift control

Voltage fed-current fed

ABSTRACT

Among the DC-DC converters, an isolated bidirectional dual active bridge converter is a core circuit for high-frequency power converters in distributed energy system applications. These high-frequency power conversion systems attract academia and industry due to various advantages, such as high-power density, less weight, reduced noise, high efficiency, low cost and high reliability. First, the importance of power electronic converters in modern-day life is introduced. Second, a topological overview of voltage-fed and current-fed isolated bidirectional dual active bridge converters is presented with their importance in integrating hybrid power sources. Third, switching modes of isolated bidirectional DC-DC converters are also presented with a degree of freedom of control. Forth, performance evaluation of voltage-fed and current-fed isolated bidirectional converters has been presented with an example. Their suitability in integrating fuel cells and photovoltaics with energy storage systems in low to medium-power applications is presented.

This is an open access article under the [CC BY-SA](https://creativecommons.org/licenses/by-sa/4.0/) license.



Corresponding Author:

Kiran Bathala

Department of Electrical and Electronics Engineering, National Institute of Technology Karnataka

Surathkal, India

Email: kiran0219@gmail.com

1. INTRODUCTION

Renewable energy resources are intermittent, so it is necessary to provide auxiliary energy storage systems for these resources to increase their reliability [1], [2]. In the energy sector, distributed energy systems (DES) will occupy a significant role in the future. Power from solar, windmills, microturbines and fuel cells (FC) will play a crucial role in DES. These non-conventional energy sources have no dispatch capability on their own. Adding an energy storage system as a backup source in the distributed generation system increases the reliability of the overall distributed energy resources. In the coming years, using a hybrid electric vehicle (HEV) along with the utility grid in the form of plug-in hybrid electric vehicles is guaranteed by introducing an energy storage system with long-term or short-term energy buffering capability [3]–[5]. DES requires specific PE topologies to directly convert the power to interconnect to the utility grid or consumer applications.

Power electronics can occupy a considerable part of the total capital cost of a typical distributed energy system, as shown in Figure 1 [6], [7]. The investment in PE and other capital costs occupy the same percentage, i.e., 20% and 80% of the total cost in PV and Fuel Cell applications, respectively. In wind power applications, PE and other capital investments occupy 30% and 70% of the total cost, respectively. In the micro-turbine application, the investment cost on PE and other capital is 40% and 60%, respectively. The input fuel cost is zero for PV and wind power applications among the four energy sources. The input fuel and PE costs are the lowest for PV power generation. Whereas for the fuel cell application, the additional cost for

the input fuel is high compared to the PV. The PV and FC systems produce DC power, whereas, for utility purposes, the generated power has to be converted to 1- ϕ or 3- ϕ AC power. The output power from the windmills and micro-turbine systems is AC, and the frequency is not constant, which has to be converted to 50Hz AC for utility connection.

The PE conversion systems mainly employ power frequency transformers for achieving galvanic isolation and impedance matching. However, the line or power frequency transformers reduce power conversion systems' efficiency and power density [8]. The rapid growth of distributed energy technologies and battery storage systems has raised the potential of power conversion systems as an ever-lasting key interface [9]–[15]. High-frequency transformers in place of regular low-frequency transformers have become a new trend in recent years. These HF transformers are taking power conversion to the next level with advantages such as being compact, less weight and cost. HF power conversion systems with HF transformers can also avert current and voltage waveform distortions.

Power conversion systems noise can be significantly reduced if the switching frequency is maintained more significantly than 20 kHz. The distinct feature of power electronics converters for energy storage systems (ESS) is that they must allow power flow in both directions, for both receiving powers from the grid for charging and delivering power to the grid while discharging. DC-DC power converters play a significant role in power distribution when the power is generated from renewable energy resources. In searching for HF bidirectional power flow converters, isolated bidirectional DC-DC converters (IBDCs) usually act as a core (mains) circuit. The demand that has been increasing for intermediate energy storage systems in battery units has raised the demand for the bi-directional DC-DC converter, which gives galvanic isolation apart from bidirectional power flow. Isolated bidirectional dual active bridge converters are the most suitable to transfer a large amount of power. HF isolation transformer can prevent the direct current flow path between the bridge circuits through the isolation transformer.

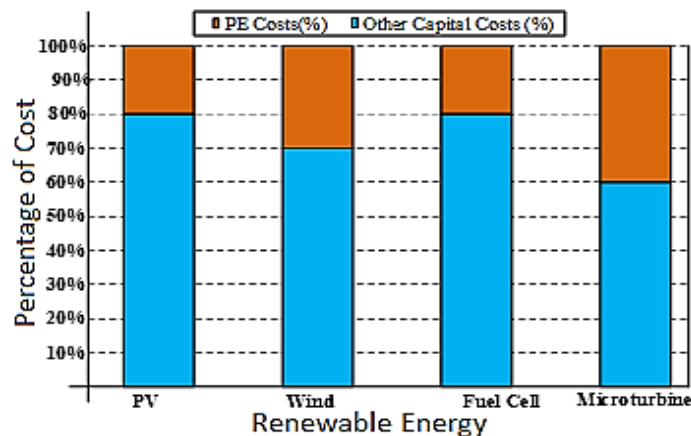


Figure 1. Investment on PE costs out of total capital costs in a DE systems [16]

Dual active bridge (DAB) isolated bidirectional DC-DC converters (IBDCs) have the highest power transmission capacity because the power transmitted is directly proportional to the number of switches in the converter. These converters can achieve soft switching easily, and power can be transmitted in both directions [17]. The circulating current is a major disadvantage and decreases the converter's efficiency [18], [19]. The decrease in efficiency increases with an increase in the difference between the switching frequency and resonant frequency. A bidirectional DC-DC converter, succeeded by an inverter, is the most general choice for storage devices. The bidirectional converters are fed from either a voltage or current source, depending on the input available and output requirement. In voltage-fed IBDCs, non-resonant IBDCs [20], [21] resonant IBDCs [22], [23] and similarly in current-fed, non-resonant [24], [25], resonant network [26]–[28] both this type of converters are discussed respectively with their merits and demerits. The resonant network helps voltage-fed, current-fed IBDC converters improve performance. Soft switching is explained with waveforms and factors influencing soft switching, and its positive and negative impacts are presented. Various types of resonant converters are presented; in terms of duty cycle, soft switching, range, extra components required and their bidirectional transition speed. Depending on the input, it needs to be pre-regulated before supplying to achieve the desired output; in such cases, a two-stage converter is needed. In two-stage converters, the importance of interleaved converters is also presented [29], [30]. IBDC converters with fewer switches are

also discussed along with applications [31], [32]. The cost of various IBDC converters is compared along with the applications.

The focus of this paper has been on various voltage and current-fed isolated BDCs topologies for low to medium-power applications and their suitability in integrating renewable energy sources with battery energy storage systems. The suitability of IBDC converters for low voltage input, such as fuel cells and photovoltaic applications, has been discussed in the following sections. For fuel cell applications, for example, two converters, i.e., voltage-fed and current-fed of exact specifications, are compared and investigated for the low voltage input applications. The impact of the degree of freedom of control (DFC) is presented by giving the power transmission and circulating power of various switching modes. DFC's influence on losses and efficiency is also presented [33], [34]. An overview of energy storage systems is also discussed [35]–[37]. This paper is scripted as follows: section 2 explains the broad classification of isolated bidirectional converters. Switching modes are explained in section 3, followed by a discussion on the importance of power electronics in distributed energy systems (DES) and the cost of various IBDC converters in section 4, and the conclusion is presented in section 5.

2. CLASSIFICATION OF ISOLATED BIDIRECTIONAL DUAL ACTIVE BRIDGE DC-DC CONVERTER TOPOLOGIES

The general block diagram with various stages of IBDC converters is shown in Figure 2, its classification details based on the type of source are shown in Figure 3 and are explained in subsections 2.1 and 2.2 respectively.

2.1. Block diagram representation of configuration

The block diagram representation of the isolated DAB bidirectional DC-DC converter is shown in Figure 2. Port-1 and port-2 can act as a source or sink depending on the direction of power flow. During the forward power flow, a DC voltage source is connected to port 1. The voltage output of this source is smoothed with the help of filters (L/C). The selection of filters is also made to convert the source as a voltage type of current type. In the case of a current source, this constant DC voltage or current is converted into AC by using a high frequency (HF) inverter. HF resonant elements are used to aid the bridge in achieving soft switching. The output of the DC-AC converter is applying to the primary of the high-frequency transformer via resonant network circuit elements. HF transformer is used to provide galvanic isolation and to scale the voltage levels up or down. The transformer's output is given to the AC-DC converter through the HF secondary side resonant network. This resonant network helps the AC-DC converter to achieve soft switching. The AC-DC converter converts HF AC into DC voltage. The secondary side filter network comprising C/L can act as a voltage/current source load at port 2. A capacitor is connected across the output terminals of the controlled (AC-DC converter) rectifier. The capacitor gets charged during the conduction period and offers low impedance to the ripple components. This capacitor discharges the stored energy during the non-conduction period; it maintains a constant voltage across the output terminals of the rectifier. So, this is named a voltage source type load.

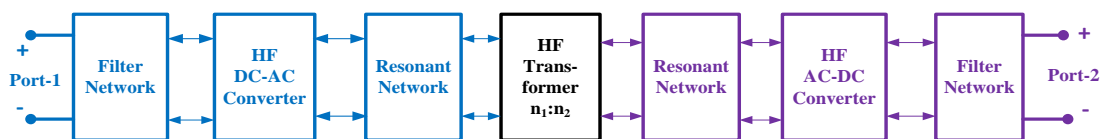


Figure 2. Block diagram representation of the isolated DAB bidirectional DC-DC converter

An inductive filter is connected in series between the AC-DC converter and the load at the filter network shown in Figure 2. Since the frequency and its inductive reactance are directly proportional, DC components offer zero impedance, and the rest are blocked. This filter stores the energy during the conduction period, and it does not allow sudden changes in the current. During the non-conduction period, the stored energy discharges through the body diode and maintains a constant current. So, it is called the current source type load. During the reverse/ discharge operation, when stored energy is fed back, or a DC supply is given at port-2, the same sequence of operation happens from port-2. In the HF AC part on either side of the HF transformer, reactive HF networks enable energy storage capability, which helps change the shapes of the switch current waveforms to reduce switching losses. The HF resonant networks are not necessarily required for a full bridge isolated bidirectional DC-DC converter because of inherent parasitic

components such as leakage, magnetizing inductance and a parasitic capacitance of practical HF transformer. These resonant networks can aid the converter in achieving higher efficiency [38], [39].

2.2. Classification

The DAB DC-DC converters, in general, are classified as one-stage and two-stage BDCs, as shown in Figure 3. Furthermore, the isolated converters are classified into non-resonant and resonant IBDCs. These converters may be fed from a voltage or current source depending on the applications and kind of input supply available. These converters are explained in this in terms of their contribution. IBDCs converters are further classified as one-stage and two-stage converters based on the number of power conversion stages. The single-stage converter is further classified as a non-resonant and load-resonant converter. These resonant converters are classified as voltage source type and current source type converters based on the type of source used. The magnetically coupled with and without DC link converters are further classified as voltage-source and current-source converters. The magnetically coupled interleaved converter has only the current source as input. The dual active bridge (DAB) converters initially started with non-resonant converters, and non-resonant DAB (NRDAB) converters with a voltage source can enable the converter to achieve high power density, reduce the switching loss through soft switching [40], [41].

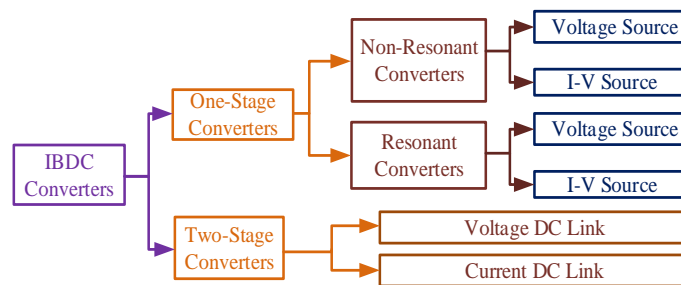


Figure 3. Classification of dual active bridge (DAB) DC-DC converters

2.3. Voltage-fed non-resonant IBDC converters

A typical structure of an isolated bidirectional dual active bridge DC-DC converter (IBDC) is shown in Figure 4. The NRDAB converter can be effectively utilized because of the symmetrical structure, and a simple control technique can be implemented. Even though the current and voltage rating of each switch is the same, the power transmission capacity of the IBDC converter is directly proportional to the number of switches. Eight switch IBDC converter power transmission capacity is double that of four switches (half bridge) IBDC converter [42]. Soft switching, zero voltage switching (ZVS) and zero current switching (ZCS) are shown in Figures 5(a) and 5(b) respectively, for the NRDAB IBDC ZVS is achieved by the junction capacitance and the magnetizing inductance of the HF transformer. NRDAB fed voltage source converter has circulating current when it is controlled by using the single-phase shift control (SPS) technique. The circulating current in NRDAB due to SPS increases with input voltage. It further leads to an increase in the peak and RMS current of the switching devices, which results in an increase in the conduction losses; hence, the efficiency of the converter reduces. To overcome the drawbacks of the SPS technique, the dual-phase shift technique (DPS) is proposed for a voltage-fed non-resonant DAB (VNRDAB) converter [42].

Conventional isolated DAB converter uses eight switches, and it needs a separate gate drive circuit. By reducing the number of switch counts, the cost of a switch and its gate driver can be saved. In the literature, a DAB converter with a push-pull topology on the primary side of the HF transformer is presented. To achieve zero voltage switching (ZVS) for the push-pull topology, an additional switch is connected on the primary side, which is fed from low voltage, and it is shown in Figure 6. On the primary side, only three switches are used when compared to conventional DAB, and this will reduce the cost of driving the circuit. Whereas, on the secondary side full bridge is used. To achieve ZVS for the converter, extended phase shift (EPS) control is used [43]. In the DAB converter with the SPS control scheme, two-level square wave voltage appears across the isolation transformer, which causes the circulating current. This circulating current can be reduced by increasing the levels of the voltage across the isolation transformer. A hybrid full-bridge isolated buck-boost converter offers three-level voltages at the primary side of the isolation transformer, and it has five variable voltage levels. The increase in voltage levels reduces the circulating current. This leads to wider voltage control in the integrated buck-boost converters. This converter offers low voltage stress, which is half of the input voltage on transformer primary side switches and offers less peak and current stress of the switching devices.

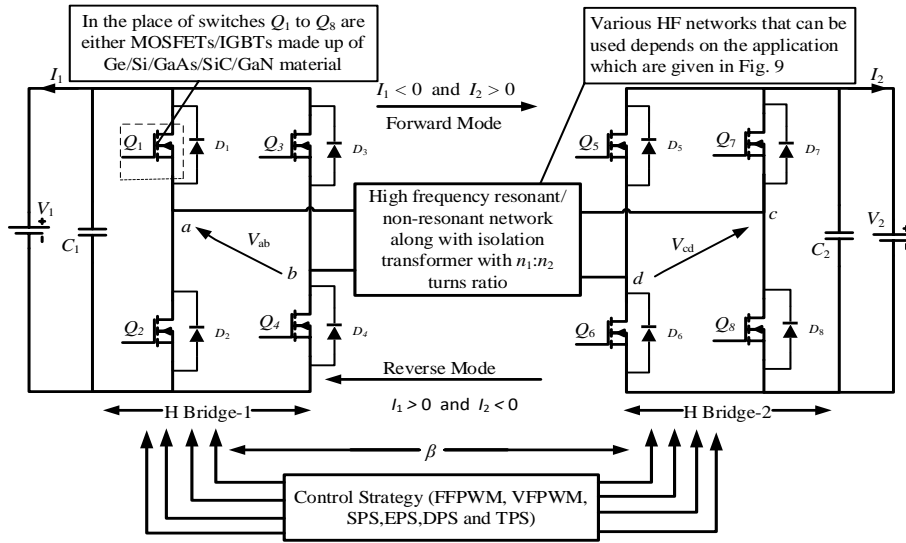


Figure 4. Typical structure of isolated bidirectional dual active bridge DC-DC converter (IBDC)

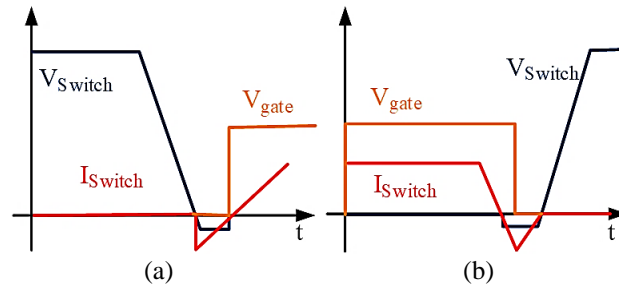


Figure 5. Typical waveforms depicting the feature of soft switching of (a) zero voltage switching and (b) zero current switching

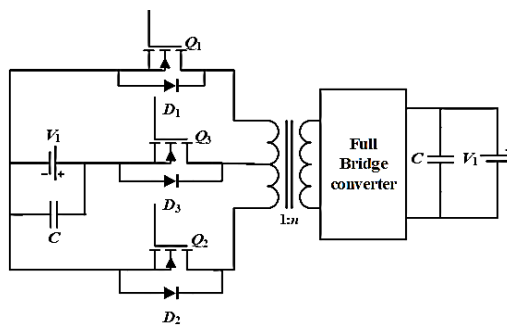


Figure 6. Improved push-pull topology [43]

A DAB converter with a hybrid bridge on the primary side and a half-bridge on the secondary side of the converter is shown in Figure 7 [44], controlled with a voltage match control technique. It is controlled with the DAB converter's extended phase shift control (EPS). This control technique is used when the overall voltage gain is double compared to its minimum input voltage to output voltage gain. This control technique offers ZVS for the six main switching devices and for the two auxiliary switches [44]. In order to accommodate many sources, the converter discussed in [45] is an appropriate choice. In an integrated buck-boost converter, to avoid the circulating current, the converter operates in boundary current mode or discontinues conduction mode [46], [47].

The DAB converters, also found in traction applications, have disadvantages such as switching noise, voltage ripple at the DC input side, quantization noise in analogue to digital converters and noise in the measuring circuits. The mechanism behind generating these noises and their impact on the DAB converter is

analyzed. To reduce the influence of these noises, the sampling frequency of the DAB converter must be different from the control frequency. To increase the performance and the dynamic behavior of power electronic traction transformer, the control frequency must be kept much higher when the sampling frequency of the DAB converter is higher than the switching frequency [48]. The IBDC converter can also be fed from multiple input sources for energy storage applications. This converter can operate with a single independent or combinational source, as shown in Figure 8. In multiple-input IBDC configuration, the multiple energy storage systems are connected for transferring the power in charging/discharging directions. This multiple-input DAB converter offers enhanced efficiency under light load conditions compared to the conventional DAB converter. This converter reduces the circulating power flow and current stress on switches, and the power transfer range can be extended easily [49]. Dual-phase shift (DPS) control scheme is used for the VNRDAB converter to improve efficiency, and the switching characteristics of VNRDAB converters are presented. The power loss model to estimate the energy loss for each power device is developed. Analysis to have optimized efficiency characteristics across the selected range is also presented [50].

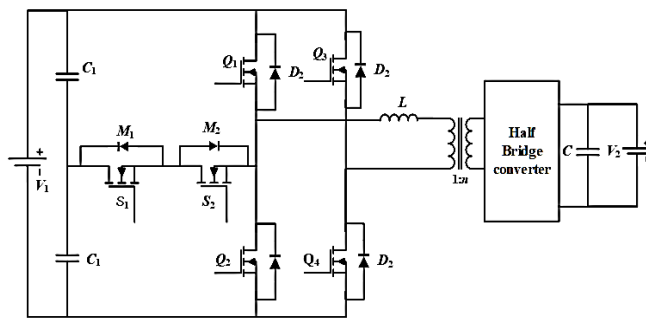


Figure 7. DAB with an auxiliary half bridge on primary side [44]

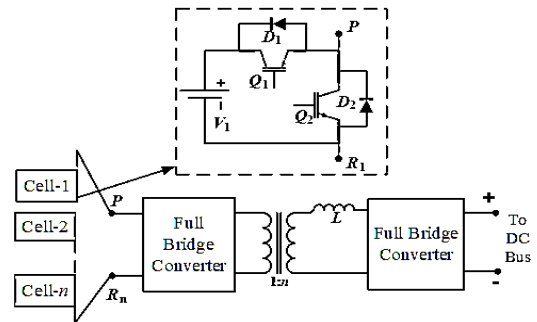


Figure 8. Multiple-input configuration of isolated bidirectional DC-DC converter [45]

Single phase VNRDAB has a lesser number of switches than three-phase VNRDAB. The current rating of switching devices in three-phase VNRDAB converter is lower. The currents in each phase of the three-phase VNRDAB converter are low compared to the single phase VNRDAB, which makes this converter more efficient. The DAB converter is provided with average current control and load current feed forward control technique to protect the circuit from overcurrent which is obvious because of voltage mode control technique [42].

Three-phase isolated bidirectional DAB converter with voltage source is presented [51]–[54]. In literature, three phase IBDC converter is compared with the single-phase voltage fed IBDC converter. Compared to single phase topology, three-phase VNRDAB converter offers higher power density. On the other side, control circuit of single phase VNRDAB is simpler compared to the three-phase topology. Three-phase topology maintains constant power between the two ports; this feature will reduce the filter size. The same three-phase converter can be operated as single-phase topology, since it can provide redundancy [55].

A modulation strategy is presented to reduce the conduction losses for the total load range of the three-phase VNRDAB converter. It increases the range of soft switching of the converter even under a large variation of voltage operations. Broad analysis of the duty cycle control is presented to improve the performance of the converter. Fast transient current control method is presented for the three-phase VNRDAB converter; it balances the transformer currents for any abrupt change in duty cycles and reduces the oscillation in DC currents [56]. The disadvantages of the VNRDAB converters, HF transformer gets saturated due to the DC component of an-asymmetrical waveform of the transformer current, in order to avoid the disadvantage additional components are required for these converters. In VNRDAB converters the effect of dead time on voltage sag, polarity reversal and unexpected phase shift in the converter is presented [43].

2.4. Voltage fed resonant IBDC converters

In voltage source resonant isolated bidirectional DC-DC converters, apart from the magnetizing inductance, a capacitor is connected in series with the transformer. In these resonant converters, along with junction capacitance, a series LC resonant network is also present, as shown in Figure 9(a). Two methods are proposed to analyze a dual active bridge series resonant converter. AC equivalent circuit analysis is carried out based on the type of load. In the first method, a voltage-source type of load is taken.

In the second method, a controlled rectifier with resistive load is considered. For these two methods, a detailed analysis is presented. Soft switching is achieved for both sides of the dual active bridge, and the

switches on the Primary bridge have ZVS, whereas the switches on the secondary side have zero current switching's (ZCS) [23]. Compared to the non-resonant IBDC, the resonant IBDC resonant converter has additional resonant elements. These resonant elements are connected to the HF transformer, and the various resonant configurations are shown in Figure 9. These resonant elements are used to achieve soft switching for the primary and/or secondary side bridges of the HF transformer. Since the resonant elements change the waveforms of the switch currents, this feature can be used to attain reduced switching losses [50]. IBDC converters with series resonant networks [54], [60] with switchable resonance frequency and converters with resonant filters are presented [61].

A DAB converter with a symmetric LC resonant network is presented, as shown in Figure 9(b). A decoupled control scheme with a PI controller is designed to control both deep currents and resonant IBDC converters. These currents, in turn, control the magnitude of the power transfer and Phase angle between the full bridges being controlled to reduce losses by improving the soft switching of the converter. Even though the load increases due to the series capacitor, RMS currents remain low in switches and resonant tanks. Because of the two voltage source ports, bidirectional power flow control has no restrictions. At no load conditions, currents become exceedingly high. Output RMS currents become high for low-voltage applications. It is not suitable for this application because of the voltage source output. It is unsuitable for wide-range operation of voltage and power values [62].

Lee *et al.* [63] the advantages of LLC resonant converters are presented. It ensures ZVS from light load to full load, switch turn off current and switching loss are low. This resonant network also offers high voltage gain and reduces the necessity for bulk capacitors. High efficiency is possible at high input voltage and ZCS for the secondary side switches. Demerits of the LLC resonant converter include a reduction in power conversion efficiency because of the circulating power. A multi-element resonant converter can overcome the demerits of the LLC converter [64]. In symmetric resonant LLC , a network is used, as shown in Figure 9(b), for the LV DC distribution system. Inductors are placed on a single core, reducing the converter's size. It offers ZVS for the primary switches and soft commutation for the secondary switches. The voltage stress on the switches was reduced without any snubber components. Intelligent digital control systems regulate the voltage at the output side and simultaneously control the power in both directions [57]. Figure 9(c) shows the type-11 LLC resonant tank, sharing features closer to the CL parallel-type resonant converter. The load comes in parallel with the resonant network $C_s-L_m-L_s$ during the resonant stage. The main difference between Type-4 and type-11 is that the latter type offers higher voltage gain than the former at the same switching frequency. A modified LLC resonant topology is presented with a control scheme, and all switches achieve soft switching. This LLC topology, shown in Figure 9(c), offers better performance compared to the series resonant converter, has reduced circulating current, turn-off losses and improved conversion efficiency compared to the conventional IBDCs. The control scheme used for modified LLC topology automatically changes the direction of power at the output without interruption. This feature makes this converter more suitable for energy storage applications [39]. Two different LLC resonant networks are presented, as shown in Figures 9(d) and 9(e). Figure 9(d) shows that it is closer to regular LC series resonant converter because of the $L_s C_{s1}$ resonant stage. Type-4 LLC resonant network shown in Figure 9(e) is extensively viewed as a band filter with the series-parallel type of resonant network. Figure 9(f) shows LCL resonant network, an extra inductor (L_s) connected across the HF transformer's secondary side. This inductor is used in the place magnetizing inductor, whereas leakage inductance of the transformer is observed as part of the series resonant inductor (L_p) on the transformer's primary [59].

This LCL bidirectional DAB converter used a ZVT circuit to achieve soft switching for one of its switching devices under light load conditions. This LCL DAB converter is controlled by using a modified gating scheme. Table 1 shows different converters and their soft-switching solutions. Voltage source dual active bridge series resonant converter with a variable frequency power control scheme is presented. An out-of-phase relationship between tank current and bridge voltages causes the switching loss (due to hard switching) in converters. This out-of-phase relationship also induces conduction loss due to increased circulating current, which increases the root-mean-square value of the tank current. To achieve the soft switching, minimum tank current operation is given to establish an in-phase relationship between resonant tank current and secondary voltage of the transformer. A series resonant DAB converter is presented to achieve minimum-tank-current operation along with full-range soft-switching. In the design process, parasitic capacitance is considered due to the non-ideal behavior of switching devices. Dead time is estimated for achieving complete soft switching [65]. DAB converter with various operation modes is given with their respective boundary conditions. These conditions are distinguished by phase-shift angle and load conditions. The expression for ripple at the output voltage was derived. The dead-band effect and safe operational area are further investigated. The relations between output power, leakage inductance, and switching frequency are also presented [66].

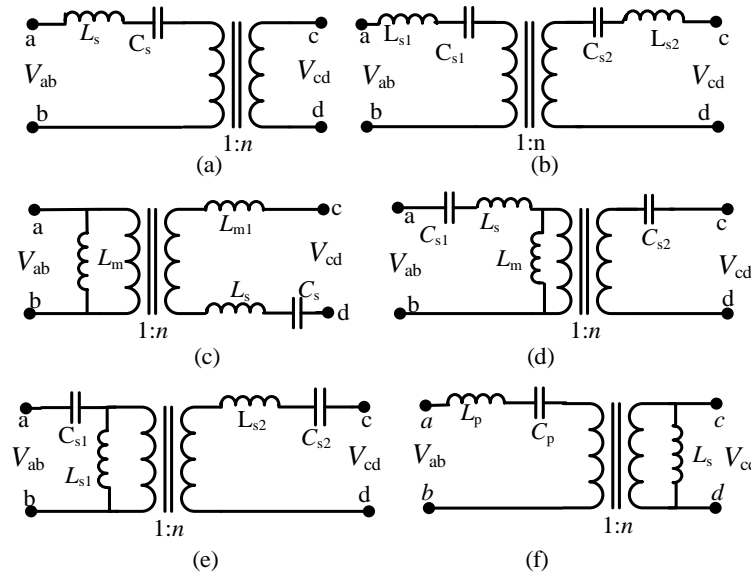


Figure 9. Various resonant networks of IBDCs (a) series resonant (SR) [23], (b) symmetric SR [57], (c) *LLC* resonant tank [39], (d) type-4 *CLLC* [58], (e) type-11 *CLLC* resonant tank [58], and (f) *LCL* resonant tank [59]

Table 1. Different soft switching solutions [17]

S. No.	Type of converter	Resonant Network (RN)	Switching Scheme	Duty ratio	Soft-switching (SS)	SS range	Additional component	Bidirectional transit-on speed
1	Conventional type	No	Phase-shift modulation	50% duty ratio for all switches	ZVS for few switches	Narrow	No	Fast
2	<i>LC</i> -RN	Series RN	Phase shift modulation	50% duty ratio for all switches	ZVS for few switches, ZCS for secondary switches	Narrow	A capacitor	Fast
3	<i>CLLC</i> -asymmetric RN	Series-parallel RN	Frequency modulation	50% duty cycle for inverter switches, additional resonant signals for rectifier switches	ZVS for inverter switches, ZCS for rectifier switches	Wide	Two capacitors and an inductor	Slow
4	<i>CLLC</i> -symmetric RN	Series RN	Frequency modulation	50% duty ratio for inverter switches, turn-off for rectifier switches	ZVS for inverter switches, soft commutation for rectifier switches	Wide	Two capacitors and an inductor	Slow

In the literature, the forward and reverse modes of the converters are fed from the voltage source. But, depending upon the application, IBDCs can be fed from the current source/voltage source. This type of single-phase current source converter offers a high step-up ratio because of its integral boost operation [20], [67] which is presented in the following subsection.

2.5. Current fed non-resonant IBDC converters

A Current source converter can have high power transfer capacity and requires low gate drive requirement. The highly efficient current-fed IBDC converter is presented for the FC EV driving system, and it is shown in Figure 10. This topology offers a smaller number of switches. Hence, the cost of the gate drive requirement is reduced to half compared to a conventional DAB converter. Coupled inductors reduce the converter's size, increasing the converter's power density [24]. A snubber less line commutated current fed isolated bidirectional dual active bridge (CIBDC) converter is presented for fuel cell applications. The modulation technique used in this CIBDC offers a natural commutation, ZCS, as shown in Figure 5 for the primary and ZVS for the secondary switches. Because of the natural commutation and soft switching, losses are reduced significantly. These features make this topology suitable for fuel cell-based EV applications. The modulation approach suggested is simple and easy to implement.

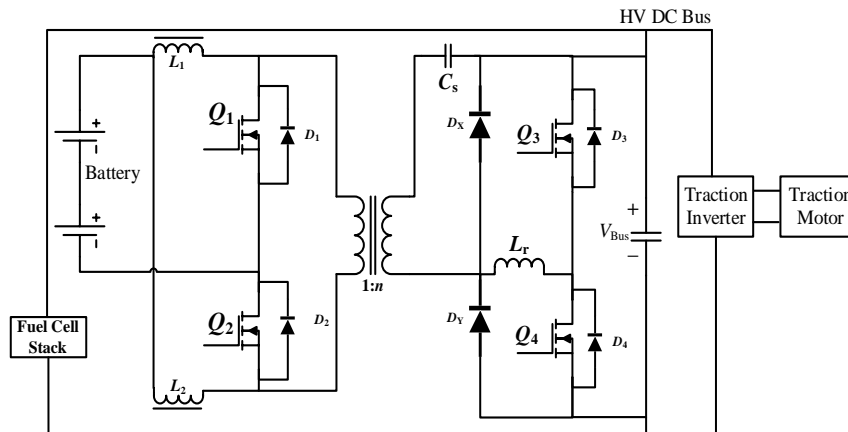


Figure 10. A bidirectional DC–DC converter for fuel cell electric vehicle driving system [24]

The circuit is modular and easily interleaved to extend the power range for high-power applications [68]. Using the merits of topology presented, interleaved topology with two cells for ESS as voltage doubler in FC electric vehicles applications is shown in Figure 11. This topology offers fewer switching losses and allows HF switching with compact size and higher power density. The voltage and current-fed IBDCs are full bridge converters [69]–[71], it [71] has two cells with four bridges and two HF isolation transformers, one cell can transfer 50% of power in the case of failure of another cell. Voltage-fed current double converters [72], [73] current source push-pull converters [58], IBDC converters using an asymmetrical PWM modulation scheme can be seen with more than one switch [74]–[76]. These converters can be applied for high-power applications. A current source IBDC converter is presented with inductors on the DC low voltage side. These inductors are placed on a single core to reduce the core losses and size and increase the power density [77], [78]. A modulation scheme controls the switches to achieve soft switching throughout the load range. This work also presents the ZVS for the LV side bridge when the duty cycle is less than 50% [77].

In the literature, a 1kW current source isolated bidirectional converter is presented. In this work, dual PWM plus double phase shift control technique is used to reduce circulating current. So, the RMS leakage current, peak current and conduction losses are reduced. To achieve soft switching, respective conditions for the switching devices are also derived. CIBDC converter is presented for low-voltage battery applications. A modulation scheme is used to control the converter to overcome the low-efficiency performance, especially at light loads [79]. This control scheme also improves efficiency for a wide load range on a variable input voltage. The proposed control scheme offers the ZVS and flexibility in the degree of freedom of control, making these more suitable for battery storage applications. A comparative analysis is carried out among the conventional and proposed control schemes, and the benefits of the control scheme with respect to conduction loss of the switches and core loss of the inductor are presented. To reduce the magnetizing inductance of an of an isolation transformer for a CIBDC converter, a mathematical design approach is presented. This design shows the least possible magnetizing inductance, which is sufficient to maintain the circulating current to achieve ZVS operation [28].

The voltage source and current source type under non-resonant converters, the voltage source type achieve more effective converter utilization. The advantage of current-fed converters is less peak switch current because of the reduced circulating current. Hence, the transformer KVA rating and turn ratio can be minimized. In VNRDAB converters, the power transfer capability is limited by increasing the switching frequency and leakage inductance. The current source can enable the parallelization of converters easily, and the current ripple becomes low. Other advantages of current source converters are high step-up ratio and multiport interface capability, and wide input voltage range operations. One of the disadvantages of CIBDC converter is the unequal distribution of the current stress within the common legs due to the unsymmetrical structure of the converter [73], [80].

A three-phase current-fed isolated bidirectional DC-DC converter (CIBDC) is compared with a voltage-fed non-resonant dual active bridge (VNRDAB), earlier offers low RMS current, zero voltage switching (ZVS) and high efficiency for the total operating range of voltage. The input ripple current is maintained low by using the interleaved topology. This configuration uses Y-Y connected transformers, which distribute the current uniformly among the three phases compared to any other transformer connections. To overcome the disadvantages of the non-resonant IBDC converters, resonant IBDC converters are proposed [81].

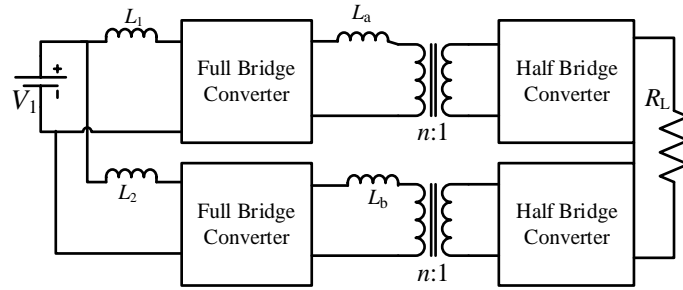


Figure 11. Interleaved current-fed IBDC with FB on primary and HB on secondary [71]

2.6. Current fed resonant IBDC converters

In resonant current source type converters, the parallel resonant converter is suitable for the low value of output voltages and high value of output currents. When the load decreases, the current through the resonant tank and switches does not reduce. Therefore, it is less suitable for wide-range voltage and power applications. The efficiency of the converter reduces because of the hard-switching operation of the switches. A modulation scheme for the series load-resonant current fed isolated bidirectional converter (CIBDC) is presented, which achieves soft switching and reduces the circulating power. This modulation scheme produces a voltage drop across the capacitor, which is connected in series with an isolation transformer to achieve soft switching even when the input or output voltage doubles comes into the scenario whenever the input or output voltage becomes [82]. A current-fed dual active bridge converter with a series resonant converter for low voltage applications, i.e., PV and FC, are presented, and it has partial soft switching. For energy storage applications, LLC resonant current-fed DAB converter is presented with complete soft switching, and inductive elements are mounted on a single core. This makes the whole converter compact because of utilizing a single core [73].

A current fed with PWM controlled bidirectional series resonant converter is presented for energy storage applications, and it is shown in Figure 12. Voltage regulation for a wide range of voltage is achieved with the PWM control technique. Soft switching (SS) for all the switches is achieved for a wide range. The design of inductive elements is made easy by choosing the switching frequency nearer to the resonant frequency. Fixed frequency-controlled voltage and current source dual active bridge converter achieved wide range soft-switching while maintaining higher efficiency compared to voltage-fed PWM converters [78]. The value of snubber capacitance across the switch influences the value of minimum current flowing through the leakage inductance of the transformer for achieving SS when the switch turns off. The value of snubber capacitance and minimum current through the leakage inductor required to achieve soft switching are directly proportional. When the winding resistance of the transformer is negligible, if the magnetizing inductance (L_{mag}) decreases, then it results in low transformer utilization and loads current will be lagging, which is a precondition for zero voltage switching (ZVS) [83]. The influence of L_{mag} on the SS region of operation is shown in Figure 13.

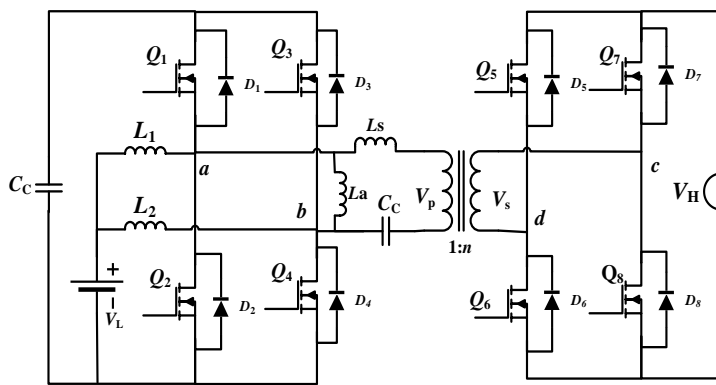


Figure 12. Current fed series resonant IBDC [78]

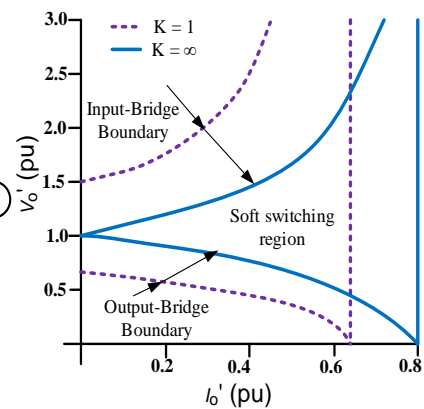


Figure 13: Impact of transformer L_{mag} on the SS region of operation

2.7. Two stage converters

In two-stage converters, the supply voltage is pre-regulated or transformed with the help of switched capacitor at the first stage. In the second stage, fine regulation of output voltage takes place with a high-frequency magnetic element; the block diagram of the two-stage converter is shown in Figure 14. They are the voltage DC-link on the low voltage side and the current DC-link on the high voltage side used to further differentiate the converter topologies. Two circuit configurations, parallel and series-parallel, are investigated with advantages and disadvantages. An intermediate DC voltage link is used to the energy storage system interface, which must have the functions of a bi-directional (two quadrant) converter connecting two voltage type sources with significantly different voltage values [84].

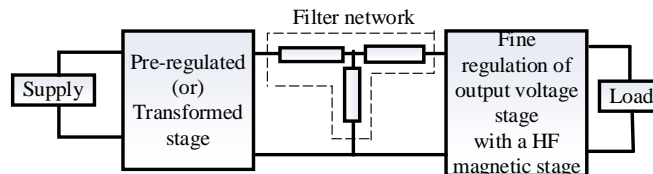


Figure 14. Block diagram representation of two stage converter shown on the output voltage-output current plane [85]

The available designs of hybrid vehicles include a BDC between the voltage bus and the energy storage system. A bidirectional DC-DC converter is used between the DC voltage bus and the Energy storage system (ESS). DC voltage is used to run the motor in hybrid vehicles, and a current-fed full bridge IBDC with an integrating buck converter is given. This topology is useful where the capacitors are used to hold the high voltage [86]. A three-phase interleaved converter is presented to integrate a low-voltage fuel cell, ultra-capacitor and load, as shown in Figure 15. This converter is a solution to convert energy by integrating a fuel cell (FC) and an ultra-capacitor (UC). Since it is a bidirectional power converter, it is possible to consume and supply ripple-free current from FC and UC. Because of the interleaved feature of the components, the current rating at input increases without parallel connection. Input filter inductors are coupled with a single core, reducing the core number and current ripple and increasing the converter's efficiency [80].

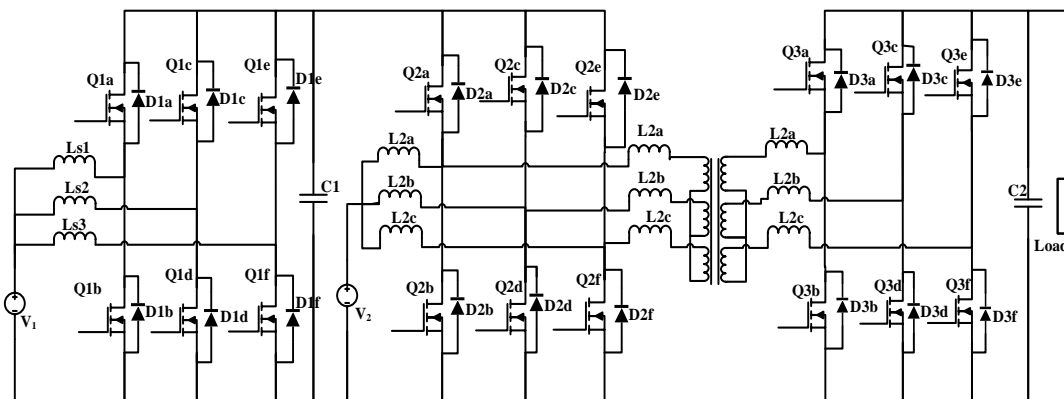


Figure 15. Interleaved three-port three phase converter for high power applications [80]

2.8. Isolated bidirectional DC-DC converters with low switch count

Isolated converters with a lower number of switches are shown in Figure 16. The converter shown in Figure 16(a) is a hard-switched fly-back converter. This operates in both forward and reverse modes of operation in continuous conduction mode. This converter is observed from the conventional fly-back converter [31]. The fly-back converter is equipped with an auxiliary circuit and is operated with soft switching. It has three switches, as shown in Figure 16(b) and is operated in zero current switching to reduce the losses, which ultimately increases the converter's efficiency [31]. This converter has input, output voltage and power of 24 V, 12 V and 50 W, respectively. This converter achieves 83% efficiency; it is 10% less than the hard-switched converter shown in Figure 16(a). The integrated Cuk converter can be seen in Figure 16(c). This magnetic integration gives various advantages; by optimizing the switching frequency. Other advantages of magnetic integration are more power density, less cost, low noise, capacitive filter requirements at both ends

can be minimized, and operating frequency can also be minimized [87]. This converter achieves an efficiency of 86% in forward mode and 76.74% in the reverse mode of operation.

A Zeta converter with galvanic isolation and two switches is shown in Figure 16(d). This converter overcomes the disadvantage of traditional Zeta converter; high voltage stress on the switches caused by the transformer leakage inductance and switching device body capacitance. This converter has an input, output voltage and power rating of 60V, 10V and 30W, respectively [88]. This converter achieves a peak efficiency of 88%. An IBD current-fed converter is presented in Figure 16(e). This converter consists of a flyback transformer with coupled inductors L_{FBp} and L_{FBs} . A push-pull transformer with coupled magnetics L_{PPp1} , L_{PPs1} and L_{PPp2} , L_{PPs2} . Four bidirectional current-controlled, unidirectional voltage switching devices are present in the converter. This converter is fed from 80V input and has 160V output with a power rating of 800W. This current-fed converter offers less input current ripple on either side of the converter. It offers high efficiency with fewer passive components [89].

A push-pull converter derived from the dual active bridge is shown in Figure 16(f). This converter uses coupled inductors instead of separate inductors. It also consists of a forward circuit with a half-bridge. It requires less gate drive circuitry because it uses a smaller number of switches. The input, output voltage and power ratings are 40V, 200V and 500W, respectively. All switches are operated with soft switching, i.e., zero voltage switching [32]. This converter has a maximum efficiency of 92.5%. Isolated bidirectional DC-DC converters with low switch counts have a narrow voltage gain range. These converters are applicable for low and medium-power applications.

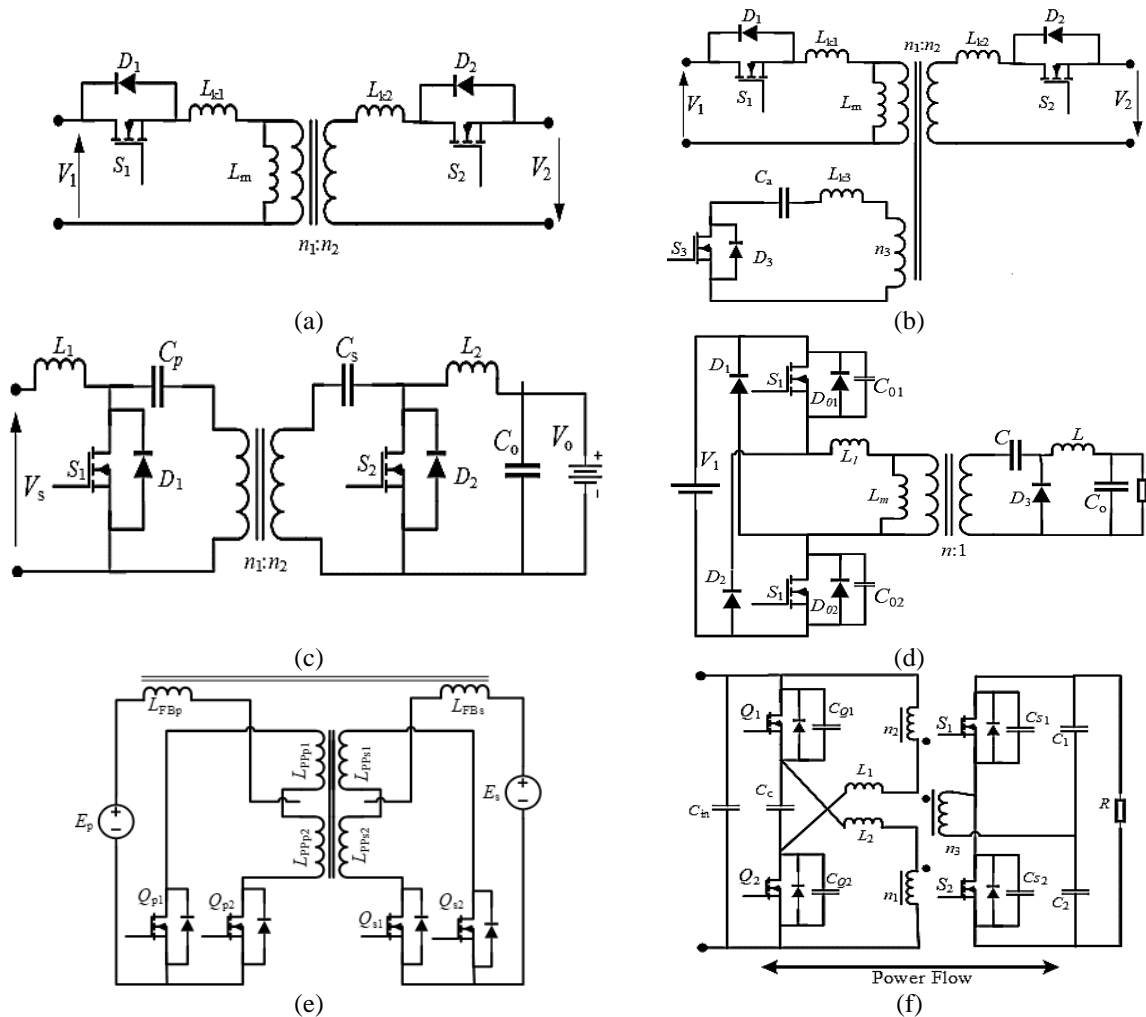


Figure 16. IBDCs with low switch count: (a) hard-switched bidirectional fly-back converter [31], (b) A ZCS bidirectional fly-back converter [31], (c) integrated bidirectional cuk converter [87], (d) isolated two-transistor zeta PWM dc-dc converter [80], (e) current fed fly-back push-pull DC-DC converter [89], and (f) push-pull forward half bridge bidirectional DC-DC converter [32]

3. SWITCHING MODES OF IBDCS

This section, it is explained the results of the research and, at the same time, is given a comprehensive discussion. Results can be presented in figures, graphs, tables and others that make the reader understand easily. The discussion can be made in several sub-sections. Switching modes of IBDCs plays an important role in controlling the power flow in both directions (i.e., forward/charging or backward/discharging). The degree of freedom of control (DFC) decides the efficiency of the control scheme [90]. As DFC increases, efficient control and conversion of power are possible. The few control schemes for IBDCs are described in subsections 3.1, 3.2, 3.3 and 3.4. The switching pulses, typical voltage, and current waveforms for the schemes are shown in Figure 17.

3.1. Single phase shift control (SPS)

The single-phase shift control (SPS) control technique is the simple and most preferred technique for isolated bidirectional dual active bridge converters. In this technique, diagonal switch pairs in two bridges are turned on to produce square waveforms having a 50% duty ratio for the respective switches. The square waveforms on either side of the isolation transformer have a phase difference; the leading voltage side bridge delivers the power to the lagging voltage bridge side of the transformer. Only a phase-shift ratio (or angle) 'd' is chosen as freedom of control by adjusting 'd' power between the bridges is controlled. Typical waveforms of the DAB converter with SPS control are shown in Figure 17(a). For voltage source non-resonant converters (VNRDAB), this SPS technique has the disadvantages such as circulating current and reactive power. These problems cause high peak current and high-power loss [91]. The other disadvantages are that the range of ZVS is limited, and current stress is more when the transformation ratio of the transformer is not near unity. This control technique is less suitable for a wide range of voltage variation applications, and it gives a maximum efficiency of 88 to 92% for various IBDCs. The expression for the power transmission and circulating power under the SPS control scheme is given in (1) and (2).

$$P_{tr} = \frac{V_1 V_2}{2nL f_s} d(1-d) \quad (1)$$

$$\text{Circulating Power } (P_{cp}) = \frac{V_1 V_2 [m + (2d-1)]^2}{16f_s n(m+1)} \quad (2)$$

Where 'm' is the ratio of V_1 and nV_2 , n is the transformation ratio of the isolation transformer, and L is the leakage inductance of the transformer. The maximum circulating power (P_{cp}) flow occurs at $m=1$, which is approximately 25% of maximum power transmission ($d=0.5$) CP flow will be more than 25% when $m > 1$ & $d=0.5$; ($P_{base} = \frac{(nV_2)^2}{8f_s L} (3m-1)$). $P_{(pu)} = d^2$, concludes that the P_{cp} exists in both input and output voltage ends for the entire power transmission range [92].

3.2. Extended phase shift control (EPS)

The EPS control technique is the improved version of the SPS technique, shown in Figure 17(b). This technique turns on the diagonal switch pair in one bridge, and another diagonal switch pair is turned on with an inner phase shift ratio. The output voltage at the DC-AC converter is a three-level square wave voltage, and the voltage at the input of the AC-DC converter is the two-level voltage with a 50% pulse width. This technique offers zero-level voltage on the primary side and three-level voltage, as shown in Figure 17(b); this reduces the circulating power by making the reverse flow of current zero. By comparing the EPS technique with the SPS technique, only a phase-shift ratio (or angle) 'd' is present in SPS. In the EPS scheme, the outer phase-shift ratio 'd₁' and inner phase-shift ratio 'd₂' are chosen as freedom of control. Outer phase shift ratio 'd₁' controls the direction and magnitude of power.

Inner phase-shift ratio d_2 is used to control the circulating power flow and increase the range of ZVS [91]. This control technique in a non-resonant voltage source converter efficiently regulates the power level. This scheme increases the efficiency and dynamic performance under a wide range of input voltage variations and even under the disturbance in a load [93]. The power transmission and circulating power (P_{cp}) under this scheme are expressed in (3) and (4).

$$P_{tr} = \frac{V_1 V_2}{2nL f_s} [d_2(1-d_2) + \frac{d_1}{2}(1-d_1-2d_2)] \quad (3)$$

$$P_{cp} = \frac{V_1 V_2 [m(1-d_1) + (2d_2-1)]^2}{16f_s n(m+1)}; m > \frac{(1-2d_2)}{(1-d_1)} \quad (4)$$

when $m \leq \frac{(1-2d_2)}{(1-d_1)}$, P_{cp} is zero.

The P_{cp} in SPS and EPS is the same when $d_1 = 0$, due to additional phase shift ' d_1 ' EPS reduces the circulating power by keeping the same power transmission as the SPS technique. The EPS control scheme can transfer more power than SPS when $0 \leq d_2 < 0.5$. This can achieve an efficiency of 92.5% [92].

3.3. Dual phase shift control (DPS)

The DPS control technique is an improved version of the EPS scheme; the operational waveforms of the DPS scheme are shown in Figure 17(c). Compared to EPS, the diagonal switch pairs are switched with the inner phase shift ratio, and the inner phase shift ratios are equal. This switching pattern results in three-level AC waveforms on either side of the isolation transformer [13]. The implementation of the DPS technique for a voltage source non-resonant converter is presented [93]. Three schemes of control algorithms, such as single-phase shift scheme, dual phase-shift scheme and model-based phase shift control scheme, are implemented on a full-bridge non-resonant voltage source converter. The experimental results of these control schemes are compared; MPSC offers better dynamic performance, and the DPS scheme can eliminate the reactive power under light load conditions. DPS offers various advantages compared to the SPS: reduced current stress and steady-state current, an increase in efficiency and range of ZVS.

Compared to the SPS control scheme, this control scheme can reduce the voltage ripple in voltage-sourced DAB [91]. For the non-resonant voltage source converter, both SPS and DPS schemes are implemented and proposed a mathematical model to analyze current stress for the IBDC converter. This analysis showed a reduction in current stress, improved converter efficiency and increased power transfer capability. This control scheme makes the converter suitable for high voltage conversion ratio and light load conditions [94], [95]. During specific operating periods, dead band compensation can be carried out without difficulty in the DPS scheme without a current sensor. Hence, the DPS scheme is easier to carry out and improves dynamic performance. The governing equation of power transmission and circulating or backflow power are given in (5) to (13). This scheme can achieve maximum efficiency of 89 to 96.5% for IBDCs.

$$P_{tr} = \frac{V_1 V_2}{2nL f_s} \left[d_2(1 - d_2) - \frac{d_1^2}{2} \right] ; (0 \leq d_1 \leq d_2 \leq 1) \quad (5)$$

$$P_{cp} = \frac{nV_1 V_2 (3m-1)}{32f_s L (m+1)} [m(1 - d_1) + (2d_2 - d_1 - 1)]^2 \quad \text{at input; } 0 \leq d_1 \leq d_2 \leq 1 \quad (6)$$

$$P_{cp} = \frac{nV_1 V_2 (3m-1)}{32f_s L (m+1)} [m(1 + d_1 - 2d_2) + (d_1 - 1)]^2 \quad \text{at output; } d_1 \leq 1 - 2d_2 \left(\frac{1}{1+m} \right) \quad (7)$$

$$P_{cp} = 0; d_1 > 1 - 2d_2 \left(\frac{1}{1+m} \right) \quad (8)$$

$$P_{tr} = \frac{V_1 V_2}{2nL f_s} (1 - d_1 - \frac{d_2}{2}) d_2; (0 \leq d_2 < d_1 \leq 1) \quad (9)$$

$$P_{cp} = \frac{nV_1 V_2 (3m-1)}{32f_s L} \left[\frac{4md_2^2 + \frac{1}{k-1} [m(1 - d_1) + d_1 - 2d_2 - 1]}{[m(1 - d_1 - 2d_2) + (d_1 - 1)]} \right]; d_1 \leq 1 + 2d_2 \left(\frac{1}{1-m} \right) \quad \text{at input} \quad (10)$$

$$P_{cp} = \frac{nV_1 V_2 (3m-1)}{32f_s L} mD_2^2; d_1 > 1 + 2d_2 \left(\frac{1}{1-m} \right) \quad (11)$$

$$P_{CP} = 0; d_1 > 1 + 2d_2 \left(\frac{1}{1-m} \right) \quad (12)$$

$$P_{CP} = \frac{nV_1 V_2 (3m-1)}{32f_s L (m-1)} \left[\frac{4md_2^2 + \frac{1}{m-1} [m(1 - d_1) + d_1 - 2d_2 - 1]}{[m(1 - d_1 - 2d_2) + (d_1 - 1)]} \right] d_1 \leq 1 + 2d_2 \left(\frac{1}{1-m} \right) \quad \text{at output} \quad (13)$$

3.4. Triple phase shift control (TPS)

This control scheme is a better version of DPS control; the TPS scheme has three degrees of freedom of control. The diagonal switch pairs are turned on for this control scheme with an inner phase shift ratio in two full bridges. Here the inner phase shift ratios are unequal, and typical operational waveforms are shown in Figure 17(d). Most of the research on the TPS scheme focused on utilizing the converter in an optimum operation [96], [97]. This technique mainly focuses on the optimized zone of operation. Power transferred from source to load [98], [99] is given by (14) to (17).

$$P_{tr} = \frac{nV_1V_2}{nf_r} [(1 - d_1 - d_3) + T(1 - d_1 - d_2 - d_3)] \tag{14}$$

Circulating power (P_{cp})

$$P_{cp} = \frac{nV_1V_2}{16f_sL(m+1)} [(1 - 2d_3 - d_2) - (1 - d_1)]^2 ; d_3 \leq \min [m(1-d_1)+2d_3 - 1, \frac{m(2d_3+d_1-1)+1}{(1+2m)}] \tag{15}$$

$$P_{cp} = \frac{nV_1V_2}{16f_sLm} \{4m(d_3 - d_2)[(1 - d_2) + m(d_3 + d_1 - d_2 - 1)] - [(1 - d_2) + m(2d_3 - 2d_2 + d_1 - 1)]^2\}; \frac{m(2d_3+d_1-1)}{(1+2m)} < d_2 \leq [1+m(2d_3+d_1-1)] \tag{16}$$

$$P_{cp} = 0; m = \frac{V_1}{nV_2} \leq -\frac{(d_2+d_3-2d_1-1)}{(1-d_1)} \tag{17}$$

Where d_1, d_2 and d_3 are the phase shifts represented in Figure 17(d). Practical application point of view, the SPS, EPS, DPS and TPS control scheme offers one, two, two and three control degrees, respectively. So, the TPS scheme is a complex scheme to carry out. For the EPS scheme, the operating states of both full bridges must be modified when the voltage conversion states or power flow directions are modified. SPS scheme has low efficiency at light loads, low range of soft switching, and circulating current. Hence, the DPS scheme can be chosen as an optimal scheme for big-scale practical implementation from the difficulty level and performance. However, TPS can achieve an efficiency range of 96 to 97.8% for the IBDC converters [34], [49].

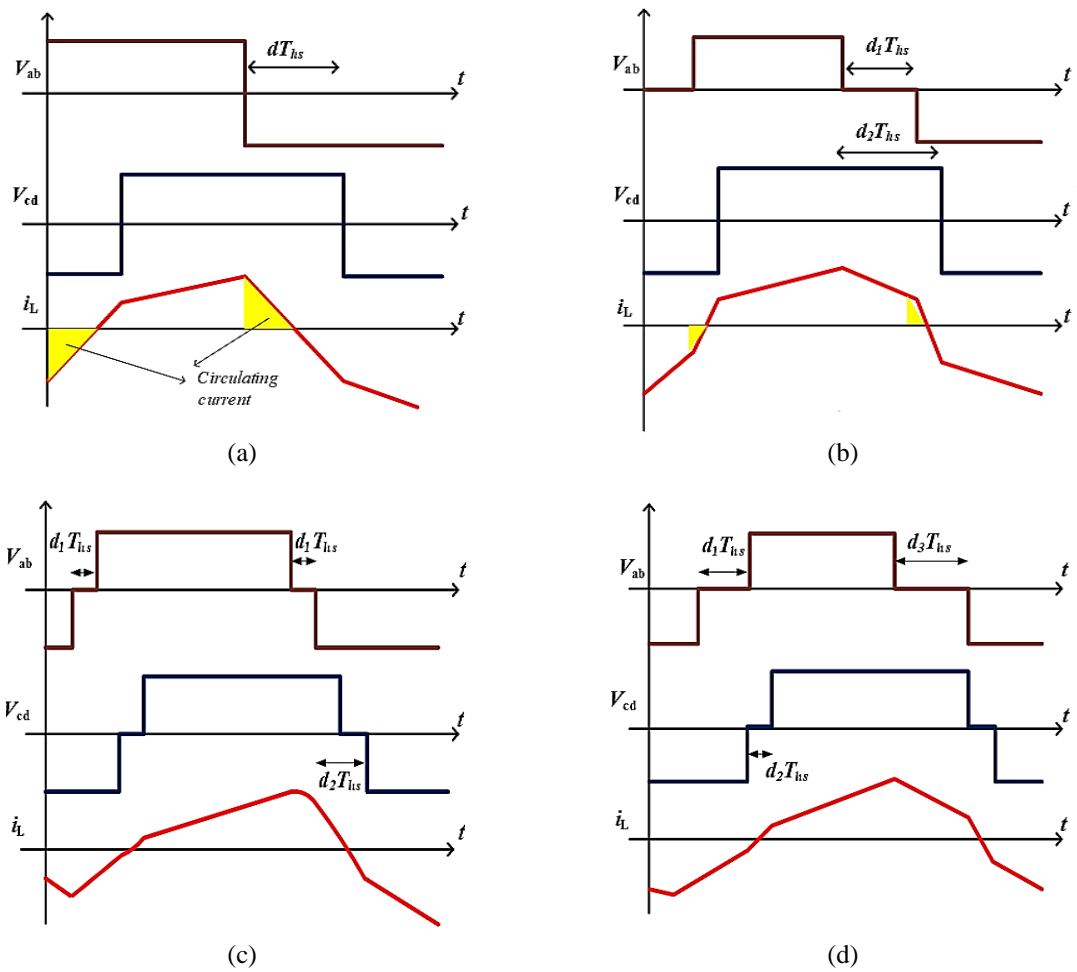


Figure 17. Typical operating waveforms of different control schemes: (a) SPS control, (b) EPS control, (c) DPS control and (d) TPS control [17]

4. DISCUSSION

In non-resonant IBDC DC-DC voltage-fed converters, non-inductive power will appear when SPS controls it. Even though the SPS technique offers less complexity in implementation, it is inefficient in reducing reactive power. In place of SPS, DPS can reduce the circulating power. DPS have two degrees of control (' d_1 ' and ' d_2 '), whereas it is one (' d ') for the SPS technique and is shown in Figures 17(a) and 17(c). The degree of freedom control can enable switches to operate in soft switching (ZVS/ZCS). The factor affecting the ZVS can be seen in Table 2. ZVS and ZCS operate the converter in lagging and leading power factor operation, respectively, as shown in Figure 5. Voltage-fed IBDC converters can maintain square wave voltage across the isolation transformer without voltage spikes. The degree of freedom of control (' d_1 ', ' d_2 ', and ' d_3 ') is three for the TPS technique, which is complex for practical implementation, and it is shown in Figure 17(d). This technique for voltage-fed IBDC converter gives less circulating power compared to the former three techniques (SPS, EPS and DPS) [100], [101].

In voltage-fed IBDC converters, efficiency increases with the degree of freedom of control; TPS switching technique offers high efficiency. The current carrying capacity in voltage-fed IBDC converters increases with an increase in switch count, which is not valid with current-fed IBDC converters. However, in current-fed IBDC converters, due to current source and inherent boosting ability, these are best suitable for low voltage and high current applications [102].

Table 2. Factors affecting ZVS and their positive and negative effects [95]

S. No.	Variable	Positive effect	Negative effect
1	Magnetizing current	Support ZVS	More current stress and conduction loss
2	Leakage inductance	Support ZVS, by reducing the rate of reversal of the primary current	Reduces the maximum effective duty ratio; hence poor VA utilization and more conduction loss. Results in higher ringing and dissipation in the secondary rectifiers
3	T_{Delay}	Large T_{Delay} aids ZVS at light loads and affects adversely at high loads.	Large T_{Delay} reduces the effective duty ratio and is particularly undesirable at very high switching frequencies
4	Capacitance across the MOSFET- C_{DS}	Large C_{DS} aids in lossless turn-off	Large C_{DS} demands more energy to be stored in the transformer inductances, to be fully discharged, hence bad for ZVS

In resonant voltage-fed isolated bidirectional dual active bridge (IBDC) converters, soft switching is achieved easily because of the resonance. The range of soft switching is narrow in the case of non-resonant compared to the resonant IBDC converters. The magnetizing current in non-resonant converters results in more current stress and losses in conducting devices. In resonant IBDCs, a resonant tank offers nearly sinusoidal current, which results in lower current stress and losses of the conducting devices. Among the resonant IBDCs, series LC resonant have a narrow soft-switching range compared to symmetric and asymmetric CLLC resonant converters (LC, Symmetric CLLC and asymmetric CLLC are shown in Figures 9(a)-(c). In CLLC-type IBDCs, asymmetric offers ZVS for inverter switches and ZCS for rectifier switches. Symmetric resonant tank gives ZVS for inverter switches and soft commutation for rectifier switches.

4.1. Cost comparison of IBDCs

A few factors decide the quality of any power electronic converter; cost is one, along with the converter's efficiency, size and power density. The cost of various IBDC converter topologies is given in Table 3 (see Appendix), with state-of-the-art and advanced components. These advanced components (GaN switches) offer ten times smaller turn-on resistance and turn-on and turn-off times; these features lead to very less losses and allow higher energy density. Since these are designed at higher frequencies, i.e., 100kHz or higher, the size of the magnetic components becomes smaller.

4.2. Example: comparison of VFC and CFC

The IBDC converters shown in Figures 18(a) and 18(b) are fed from a voltage source and current, respectively [20]. These two converters, which are rated at 1kW of power and 288V of output voltage taken as an example. Converters are investigated to check their suitability for the low voltage fuel cell and PV applications. From Figure 19(a) and Table 4, suitable components are chosen for the converter. Since it's for LV high current application, switches are selected with low R_{on} for the primary & secondary switches. The per-unit values of Figure 19(a) are shown in Figure 19 (b). The complete losses and efficiency of the two converters are shown in Figure 19(c). It is evident from Figure 19(a) that the current-fed converter (CFC) has less peak value of current through the circuit devices, and it gives less circulating current [42], [103]. This results in less conduction loss. Switch voltages of high frequency CFC and voltage-fed converter (VFC) are seen as the same from Figure 19(a) [55], which are lower values. In the case of VFC, the voltage supplied to the battery is clamped by the capacitor.

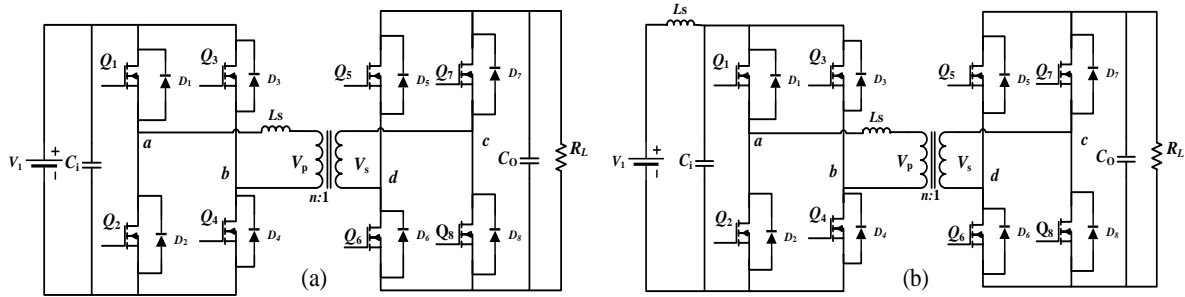


Figure 18. IBDCs (a) voltage fed dual active bridge IBDC converter and (b) current fed dual active bridge IBDC converter

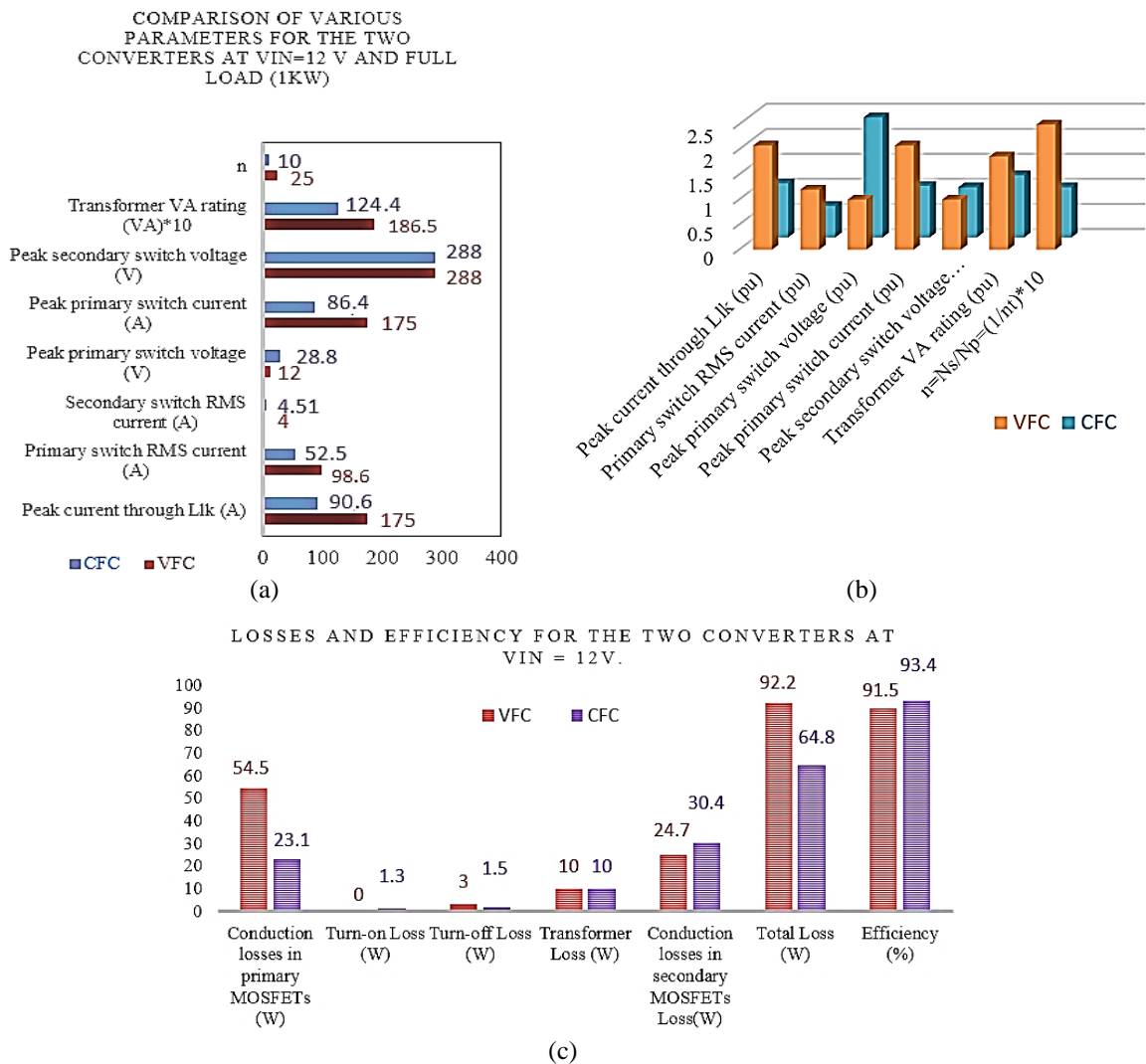


Figure 19. Comparison of VFC and CFC (a) comparison of various parameters of VSC and CSC, (b) per unit values of figure, and (c) losses and efficiency comparison of two converters

Current-fed converter (CFC) sustains higher efficiency for the same battery application, even after battery voltage fluctuates and load current decreases. It is evident from Figure 19(a) KVA rating and turns ratio required for the CFC is small compared to the voltage-fed converter (VFC); this makes the volume of the CFC converter very small compared to the VFC. Power transfer in HF Isolated power electronics systems depends on leakage inductance (L_{lk}) and switching frequency (f_s). If the turns ratio is higher, it will be challenging to design a transformer with less leakage inductance in VSC. An increase in L_{lk} and f_s can reduce the power

transfer capacity. At a given value of f_s and rated power, CFC can have a higher value of L_{lk} than VFC. For example, $P = 5$ kW VFC needs $L_{lk} = 34$ nH, whereas CFC needs 103 nH. Designing $L_{lk} = 34$ nH inductance with a higher turn's ratio is very difficult. Therefore, for a power rating less than 5 kW, CFC can supply one cell while VFC needs two or more cells with interleaving. This makes the volume of VFC higher compared to CFC of the same power rating. Because of the DC current received from the battery, CFC has better battery utilization compared to VFC. CFC can offer; high-power single cell, better battery utilization, lower peak currents, lower isolation transformer kVA ratings, less circulating currents, and improved load efficiency, which makes CFC a better choice for FC and PV applications.

In CFC, a secondary modulation scheme clamps the primary side switch voltage at a less reflected voltage. This feature enables us to use semiconductor switches with low R_{on} and voltage ratings. Table 4 shows that primary $R_{ds(on)}$ is low for VFC compared to CFC; its conduction loss is still more, as shown in Figure 19(c). It is due to the primary RMS current, which is higher than CFC, as shown in Figure 19(a). Theoretical and simulation studies gave [20] semiconductor device RMS and maximum current rise due to the increase in supply voltage, which in turn increases the conduction losses in primary side devices and lowers the converter's efficiency. For battery application, the efficiency of VFC falls due to an increase in the maximum and RMS current of the switch even after the battery is charged beyond the nominal value.

Table 4. Selected components of VFC and CFC [97]

Converter	Voltage fed converter	Current fed converter
HF Switches	IRFB3004PBF (Primary side) $V_1 = 40$ V, $I_d = 340$ A, $R_{dson} = 1.43$ m Ω	IRFB3006PBF (Primary side) $V_1 = 60$ V, $I_d = 195$ A, $R_{dson} = 2.1$ m Ω
	IPA60R385CP (Secondary side) $V_1 = 650$ V, $I_d = 9$ A, $R_{dson} = 0.385$ Ω	IPA60R385CP (Secondary side) $V_1 = 650$ V, $I_d = 9$ A, $R_{dson} = 0.385$ Ω

5. CONCLUSION

Power converters have become the most critical and inevitable components of the power electronic interface used in renewable energy generation. Isolated bidirectional dual active bridge DC-DC (IBDC) power converter topologies have been discussed, and their performance has been compared to recommend one for low input voltage distributed energy applications. Classification of voltage-fed and current-fed resonant and non-resonant IBDC converters has been made and discussed. It is found that current-fed converters offer inherent voltage-boosting capability, which makes it suitable for low-voltage PV and Fuel cell applications. Current-fed resonant converters maintain soft switching for a wide range of input voltage and load variations. A 12 V DC input, 288 V DC output and 1000 W of output power-rated voltage-fed and current-fed IBDC converters have been investigated to determine their suitability in low-voltage renewable energy applications. Based on performance parameters such as efficiency, current stress and loss of duty cycle, it is concluded that the current-fed converter topology outperforms the voltage-fed one. Power control methods that include single phase-shift, extended phase-shift, dual phase-shift and triple phase-shift controls have been discussed. Single phase-shift control is easier to control and implement while triple phase-shift control is efficient but complex to implement in IBDC converters in renewable energy applications.

APPENDIX

Table 3. Cost comparison of various topologies

No. of switched (IRF640NPBF)	Passive components capacitors(C), inductors (L)	Gate driver (ICs IR2110, HCPL2730 and capacitors)	$V_{in}/V_{out}/P_o$ Application	Estimated Cost in \$ (with state-of-the-art components)	Estimated cost in \$ (with Advanced switches (GaN) GAN063650WSA)	% η
8 [6]	C: 2 * 2200 μ F / 350 V DC L: 10.5 μ H	3*ICs IR2110 3*ICs IR2110 3*10 μ F, Electrolytic	350 V DC / 1.5 kV / 10 kW / Electrical traction	53.77	163.53	97
7 [45]	C: 2 * 880 μ F, 970 μ F / 300 V DC L: 187 μ H	3*ICs IR2110 3*ICs IR2110 3*10 μ F, Electrolytic	60 V DC / 300 V / 500 W / Energy storage	53.1	149.14	95

Table 3. Cost comparison of various topologies (continue)

No. of switched (IRF640NPBF)	Passive components capacitors(C), inductors (L)	Gate driver (ICs IR2110, HCPL2730 and capacitors)	$V_{in}/V_{out}/P_{o}$ Application	Estimated Cost in \$ (with state-of-the-art components)	Estimated cost in \$ (with Advanced switches (GaN) GAN063650WSA)	% η
8 [44]	C: 2 * 20 μ F, 2 * 400 μ F / 240 V DC L: 20 μ H	3*ICs IR2110 3*ICs IR2110 3*10 μ F, Electrolytic	120 - 240 V DC / 96 V / 1 kW / Energy storage	55.07	164.83	95
6 [104]	C: 2*10 μ F L: 2*15 μ H + core	3*ICs IR2110 3*ICs IR2110 3*10 μ F, Electrolytic	12 V DC / 150 - 400 V DC / 2 kW / FC-EV	51.78	134.1	96
8 [23]	C: 32.01 nF / 75 V AC L: 95.5 μ F	3*ICs IR2110 3*ICs IR2110 3*10 μ F, Electrolytic	110 - 130 V DC / 75 -100 V DC / 200 DC / Energy storage	53.12	162.88	95
8 [80]	C: 1410 nF, 33 nF / 630 V L: 228 μ H, 76 μ H	3*ICs IR2110 3*ICs IR2110 3*10 μ F, Electrolytic	200 - 400 V / 48 V DC / 500 W/Battery	54.42	164.18	96
8 [105]	C: 200 nF / 120 V AC L: 130 μ H, 30 μ H	3*ICs IR2110 3*ICs IR21103*10 μ F, Electrolytic	380 V DC / 220 V DC / 5 kW / Energy storage	53.77	163.53	97.8
8 [2]	C: 47 nF / 240 V AC L: 53.89 μ H, 2*400 μ H, 2*300 μ H	3*ICs IR2110 3*ICs IR2110 3*10 μ F, Electrolytic	160 - 240 V DC / 400 V DC / 1.6 kW / ESS	55.72	164.48	96
8 [69]	C: 2200 μ F / 50 V DC L: 2*164 μ H, 2*45 μ H	3*ICs IR2110 3*ICs IR2110 3*10 μ F, Electrolytic	40 - 56.4 V DC / 150 -300 / 10 kW / Hybrid ESS	55.07	164.83	94
9 [106]	C: 22 μ F / 100 V DC, 3.9 μ F / 630 V DC L: 2*40 μ H, 86 μ H, 36 μ H	3*ICs IR2110 3*ICs IR2110 3*10 μ F, Electrolytic	8 V DC / 288 V / 1.6 kW / FC	57.04	180.52	95
6 [107]	C: 56 μ F, 180 μ H / 63 V DC, 2*6.8 μ F / 400 V DC L: 10.54 μ H, 0.74 μ H, 18.56 μ H, 18.41 μ H	3*ICs IR2110 3*ICs IR2110 3*10 μ F, Electrolytic	30 - 60 V DC / 400 V / 1 kW / Energy storage	53.73	136.05	96.69
8 [106]	C: 5.6 μ F / 100 V DC, 2*3.9 μ F / 250 V DC, 10 μ F / 250 V DC L: 1.5 μ H, 11 μ H, 500 μ H, 2*10 μ H, 60 μ H	3*ICs IR2110 3*ICs IR2110 3*10 μ F, Electrolytic	600 V DC / 18 - 28 V DC / 1 kW / Battery	58.32	168.08	96.42
8 [73]	C : 0.18 μ F / 900 V AC, 12 μ F / 100 V DC, 180 μ F / 63 V DC, 1.5 μ F / 630 V DC L : 150 μ H, 3*300 μ H	3*ICs IR2110 3*ICs IR2110 3*10 μ F, Electrolytic	160 - 240 V DC / 400 V / 1.6 kW / Battery	57.02	166.78	96.49
6 [79]	C: 3.9 μ F / 630 V DC L: 9.6 μ H, 8.6 μ H	3*ICs IR2110 3*ICs IR2110 3*10 μ F, Electrolytic	22 - 4 V DC / 350 V 200W / FC	51.13	133.45	97.48
8 [44]	C: 4.7 μ F / 630 V DC L: 1.5 μ H, 16.4 μ H	3*ICs IR2110 3*ICs IR2110 3*10 μ F, Electrolytic	12 V DC / 288 V / 250 W / FC Vehicles	53.77	163.53	97.07

REFERENCES

- [1] M. Liserre, T. Sauter, and J. Hung, "Future energy systems: integrating renewable energy sources into the smart power grid through industrial electronics," *IEEE Industrial Electronics Magazine*, 4(1), 18–37. doi:10.1109/mie.2010.935861, vol. 38, no. 12, pp. 1721–1729, 2016.
- [2] T. Bi, B. Yang, K. Jia, L. Zheng, Q. Liu, and Q. Yang, "Review on renewable energy source fault characteristics analysis," *CSEE Journal of Power and Energy Systems*, vol. 8, no. 4, pp. 963–972, 2022, doi: 10.17775/CSEEJPES.2021.06890.
- [3] S. Chakraborty, B. Kroposki, and W. Kramer, "Advanced power electronic interfaces for distributed energy systems part 2: modeling, development, and experimental evaluation of advanced control functions for single-phase utility-connected inverter advanced power electronic interfaces for distribute," no. November, p. 62, 2008.
- [4] H. Wu, K. Sun, Y. Li, and Y. Xing, "Fixed-frequency PWM-controlled bidirectional current-fed soft-switching series-resonant converter for energy storage applications," *IEEE Transactions on Industrial Electronics*, vol. 64, no. 8, pp. 6190–6201, 2017, doi: 10.1109/TIE.2017.2682020.
- [5] A. A. E. B. A. El Halim, E. H. E. Bayoumi, W. El-Khattam, and A. M. Ibrahim, "Electric vehicles: a review of their components and technologies," *International Journal of Power Electronics and Drive Systems*, vol. 13, no. 4, pp. 2041–2061, 2022, doi: 10.11591/ijped.v13.i4.pp2041-2061.

- [6] Z. Tang, Y. Yang, and F. Blaabjerg, "Power electronics: The enabling technology for renewable energy integration," *CSEE Journal of Power and Energy Systems*, vol. 8, no. 1, pp. 39–52, 2022, doi: 10.17775/CSEEJPES.2021.02850.
- [7] C. Katar and C. P. Uzunoglu, "A comparative study on AC/DC analysis of an operational low voltage distribution system," *International Journal of Applied Power Engineering (IJAPE)*, vol. 10, no. 3, p. 193, 2021, doi: 10.11591/ijape.v10.i3.pp193-206.
- [8] S. Inoue and H. Akagi, "A bidirectional isolated DC–DC converter as a core circuit of the next-generation medium-voltage power conversion system," *IEEE Transactions on Power Electronics*, vol. 22, no. 2, pp. 535–542, Mar. 2007, doi: 10.1109/TPEL.2006.889939.
- [9] M. Berrehil El Kattel, R. Mayer, M. Douglas Possamai, and S. Vidal Garcia Oliveira, "Bidirectional isolated three-phase dc-dc converter using coupled inductor for dc microgrid applications," *International Journal of Circuit Theory and Applications*, vol. 48, no. 6, pp. 832–859, 2020, doi: 10.1002/cta.2795.
- [10] N. Safitri, A. M. Shiddiq Yunus, F. Fauzi, and N. Naziruddin, "Integrated arrangement of advanced power electronics through hybrid smart grid system," *Telkomnika (Telecommunication Computing Electronics and Control)*, vol. 18, no. 6, pp. 3202–3209, 2020, doi: 10.12928/TELKOMNIKA.v18i6.13433.
- [11] R. Muzzammel, R. Arshad, S. Bashir, U. Mushtaq, F. Durrani, and S. Noshin, "Comparative analysis of optimal power flow in renewable energy sources based microgrids," *International Journal of Electrical and Computer Engineering*, vol. 13, no. 2, pp. 1241–1259, 2023, doi: 10.11591/ijece.v13i2.pp1241-1259.
- [12] J. A. Adebisi, I. H. Denwigwe, and O. M. Babatunde, "Hydrogen storage for micro-grid application: a framework for ranking fuel cell technologies based on technical parameters," *International Journal of Electrical and Computer Engineering*, vol. 13, no. 2, pp. 1221–1230, 2023, doi: 10.11591/ijece.v13i2.pp1221-1230.
- [13] F. A. Syam, M. I. Abu El-Sebah, K. S. Sakkoury, and E. A. Sweelem, "Operation of biogas-solar-diesel hybrid renewable energy system with minimum reserved energy," *Indonesian Journal of Electrical Engineering and Computer Science*, vol. 28, no. 3, pp. 1203–1213, 2022, doi: 10.11591/ijeecs.v28.i3.pp1203-1213.
- [14] J. Hu, Y. Shan, K. W. Cheng, and S. Islam, "Overview of power converter control in microgrids - challenges, advances, and future trends," *IEEE Transactions on Power Electronics*, vol. 37, no. 8, pp. 9907–9922, 2022, doi: 10.1109/TPEL.2022.3159828.
- [15] N. G. F. Dos Santos, J. R. R. Zientarski, and M. L. Da Silva Martins, "A review of series-connected partial power converters for DC–DC applications," *IEEE Journal of Emerging and Selected Topics in Power Electronics*, vol. 10, no. 6, pp. 7825–7838, 2022, doi: 10.1109/JESTPE.2021.3082869.
- [16] W. Kramer, S. Chakraborty, B. Kroposki, and H. Thomas, "Advanced power electronic interfaces for distributed energy systems part I: systems and topologies," Golden, CO, Mar. 2008. doi: 10.2172/926102.
- [17] B. Zhao, Q. Song, W. Liu, and Y. Sun, "Overview of Dual-Active-Bridge Isolated Bidirectional DC–DC Converter for High-Frequency-Link Power-Conversion System," *IEEE Transactions on Power Electronics*, vol. 29, no. 8, pp. 4091–4106, Aug. 2014, doi: 10.1109/TPEL.2013.2289913.
- [18] V. Karthikeyan and R. Gupta, "Zero circulating current modulation for isolated bidirectional dual-active-bridge DC–DC converter," *IET Power Electronics*, vol. 9, no. 7, pp. 1553–1561, 2016, doi: 10.1049/iet-pel.2015.0475.
- [19] Z. Wang and H. Li, "An integrated three-port bidirectional DC–DC converter for PV application on a DC distribution system," *IEEE Transactions on Power Electronics*, vol. 28, no. 10, pp. 4612–4624, 2013, doi: 10.1109/TPEL.2012.2236580.
- [20] A. K. Rathore and U. R. Prasanna, "Comparison of soft-switching voltage-fed and current-fed bi-directional isolated Dc/Dc converters for fuel cell vehicles," *IEEE International Symposium on Industrial Electronics*, pp. 252–257, 2012, doi: 10.1109/ISIE.2012.6237093.
- [21] X. Liu *et al.*, "Novel dual-phase-shift control with bidirectional inner phase shifts for a dual-active-bridge converter having low surge current and stable power control," *IEEE Transactions on Power Electronics*, vol. 32, no. 5, pp. 4095–4106, 2017, doi: 10.1109/TPEL.2016.2593939.
- [22] D. Segaran, D. G. Holmes, and B. P. McGrath, "Comparative analysis of single- And three-phase dual active bridge bidirectional DC–DC converters," *Australian Journal of Electrical and Electronics Engineering*, vol. 6, no. 3, pp. 329–337, 2009, doi: 10.1080/1448837X.2009.11464251.
- [23] X. Li and A. K. S. Bhat, "Analysis and design of high-frequency isolated dual-bridge series resonant DC/DC converter," *IEEE Transactions on Power Electronics*, vol. 25, no. 4, pp. 850–862, 2010, doi: 10.1109/TPEL.2009.2034662.
- [24] H.-J. Chiu and L.-W. Lin, "A bidirectional DC–DC converter for fuel cell electric vehicle driving system," *IEEE Transactions on Power Electronics*, vol. 21, no. 4, pp. 950–958, Jul. 2006, doi: 10.1109/TPEL.2006.876863.
- [25] D. Sha, X. Wang, K. Liu, and C. Chen, "A current-fed dual-active-bridge DC–DC converter using extended duty cycle control and magnetic-integrated inductors with optimized voltage mismatching control," *IEEE Transactions on Power Electronics*, vol. 34, no. 1, pp. 462–473, Jan. 2019, doi: 10.1109/TPEL.2018.2825991.
- [26] Z. Qin, Y. Shen, P. C. Loh, H. Wang, and F. Blaabjerg, "A dual active bridge converter with an extended high-efficiency range by DC blocking capacitor voltage control," *IEEE Transactions on Power Electronics*, vol. 33, no. 7, pp. 5949–5966, 2018, doi: 10.1109/TPEL.2017.2746518.
- [27] Y. Shi, R. Li, Y. Xue, and H. Li, "Optimized operation of current-fed dual active bridge DC–DC converter for PV applications," *IEEE Transactions on Industrial Electronics*, vol. 62, no. 11, pp. 6986–6995, 2015, doi: 10.1109/TIE.2015.2432093.
- [28] K. Bathala, D. Kishan, and N. Harischandrapa, "Current source isolated bidirectional series resonant DC–DC converter for solar power/fuel cell and energy storage application," *IECON Proceedings (Industrial Electronics Conference)*, vol. 2021–October, 2021, doi: 10.1109/IECON48115.2021.9589693.
- [29] P. J. Wolfs, "A current-sourced DC–DC converter derived via the duality principle from the half-bridge converter," *IEEE Transactions on Industrial Electronics*, vol. 40, no. 1, pp. 139–144, 1993, doi: 10.1109/41.184830.
- [30] D. Liu and H. Li, "A three-port three-phase DC–DC converter for hybrid low voltage fuel cell and ultracapacitor," *IECON Proceedings (Industrial Electronics Conference)*, pp. 2558–2563, 2006, doi: 10.1109/IECON.2006.347822.
- [31] H. S. H. Chung, W. L. Cheung, and K. S. Tang, "A ZCS bidirectional flyback dc/dc converter," *IEEE Transactions on Power Electronics*, vol. 19, no. 6, pp. 1426–1434, 2004, doi: 10.1109/TPEL.2004.836643.
- [32] Z. Zhang, O. C. Thomsen, and M. A. E. Andersen, "Optimal design of a push-pull-forward half-bridge (PPFHB) bidirectional DC–DC converter with variable input voltage," *IEEE Transactions on Industrial Electronics*, vol. 59, no. 7, pp. 2761–2771, 2012, doi: 10.1109/TIE.2011.2134051.
- [33] H. Bai, Z. Nie, and C. C. Mi, "Experimental comparison of traditional phase-shift, dual-phase-shift, and model-based control of isolated bidirectional dc-dc converters," *IEEE Transactions on Power Electronics*, vol. 25, no. 6, pp. 1444–1449, 2010, doi: 10.1109/TPEL.2009.2039648.
- [34] S. S. Muthuraj, V. K. Kanakesh, P. Das, and S. K. Panda, "Triple phase shift control of an LLL tank based bidirectional dual active bridge converter," *IEEE Transactions on Power Electronics*, vol. 32, no. 10, pp. 8035–8053, 2017, doi: 10.1109/TPEL.2016.2637506.





- [35] S. Habib *et al.*, "Contemporary trends in power electronics converters for charging solutions of electric vehicles," *CSEE Journal of Power and Energy Systems*, vol. 6, no. 4, pp. 911–929, 2020, doi: 10.17775/CSEEJPES.2019.02700.
- [36] X. Li and S. Wang, "Energy management and operational control methods for grid battery energy storage systems," *CSEE Journal of Power and Energy Systems*, vol. 7, no. 5, pp. 1026–1040, 2021, doi: 10.17775/CSEEJPES.2019.00160.
- [37] R. B. Schainker, "Executive overview: Energy storage options for a sustainable energy future," *2004 IEEE Power Engineering Society General Meeting*, vol. 2, pp. 2309–2314, 2004, doi: 10.1109/pes.2004.1373298.
- [38] R. L. Steigerwald, "A comparison of half-bridge resonant converter topologies," *APEC 1987 - 2nd Annual IEEE Applied Power Electronics Conference and Exposition, Conference Proceedings*, pp. 135–144, 2015, doi: 10.1109/APEC.1987.7067142.
- [39] T. Jiang, J. Zhang, X. Wu, K. Sheng, and Y. Wang, "A bidirectional LLC resonant converter with automatic forward and backward mode transition," *IEEE Transactions on Power Electronics*, vol. 30, no. 2, pp. 757–770, 2015, doi: 10.1109/TPEL.2014.2307329.
- [40] P. Xuwei and A. K. Rathore, "Novel interleaved bidirectional snubberless naturally clamped zero current commutated soft-switching current-fed full-bridge voltage doubler for fuel cell vehicles," *2013 IEEE Energy Conversion Congress and Exposition, ECCE 2013*, pp. 3615–3622, 2013, doi: 10.1109/ECCE.2013.6647177.
- [41] N. Hou and Y. W. Li, "Overview and comparison of modulation and control strategies for a nonresonant single-phase dual-active-bridge DC-DC converter," *IEEE Transactions on Power Electronics*, vol. 35, no. 3, pp. 3148–3172, 2020, doi: 10.1109/TPEL.2019.2927930.
- [42] S. Shao, H. Chen, X. Wu, J. Zhang, and K. Sheng, "Circulating current and ZVS-on of a dual active bridge DC-DC converter: a review," *IEEE Access*, vol. 7, pp. 50561–50572, 2019, doi: 10.1109/ACCESS.2019.2911009.
- [43] Y. Lu, Q. Wu, Q. Wang, D. Liu, and L. Xiao, "Analysis of a novel zero-voltage-switching bidirectional DC/DC converter for energy storage system," *IEEE Transactions on Power Electronics*, vol. 33, no. 4, pp. 3169–3179, Apr. 2018, doi: 10.1109/TPEL.2017.2703949.
- [44] G. Xu, D. Sha, Y. Xu, and X. Liao, "Hybrid-bridge-based DAB converter with voltage match control for wide voltage conversion gain application," *IEEE Transactions on Power Electronics*, vol. 33, no. 2, pp. 1378–1388, 2018, doi: 10.1109/TPEL.2017.2678524.
- [45] V. Karthikeyan and R. Gupta, "Multiple-input configuration of isolated bidirectional DC-DC converter for power flow control in combinational battery storage," *IEEE Transactions on Industrial Informatics*, vol. 14, no. 1, pp. 2–11, 2018, doi: 10.1109/TII.2017.2707106.
- [46] Y. Li, F. Li, F. W. Zhao, X. J. You, K. Zhang, and M. Liang, "Hybrid three-level full-bridge isolated buck-boost converter with clamped inductor for wider voltage range application," *IEEE Transactions on Power Electronics*, vol. 34, no. 3, pp. 2923–2937, 2019, doi: 10.1109/TPEL.2018.2845308.
- [47] F. Li, Y. Li, and X. You, "Optimal dual-phase-shift control strategy of an isolated buck-boost converter with a clamped inductor," *IEEE Transactions on Power Electronics*, vol. 33, no. 6, pp. 5374–5385, 2018, doi: 10.1109/TPEL.2017.2732439.
- [48] J. Yang, J. Liu, J. Zhang, N. Zhao, Y. Wang, and T. Q. Zheng, "Multirate digital signal processing and noise suppression for dual active bridge DC-DC converters in a power electronic traction transformer," *IEEE Transactions on Power Electronics*, vol. 33, no. 12, pp. 10885–10902, 2018, doi: 10.1109/TPEL.2018.2803744.
- [49] V. Karthikeyan and R. Gupta, "FRS-DAB converter for elimination of circulation power flow at input and output ends," *IEEE Transactions on Industrial Electronics*, vol. 65, no. 3, pp. 2135–2144, 2018, doi: 10.1109/TIE.2017.2740853.
- [50] B. Zhao, Q. Song, and W. Liu, "Efficiency characterization and optimization of isolated bidirectional DC-DC converter based on dual-phase-shift control for DC distribution application," *IEEE Transactions on Power Electronics*, vol. 28, no. 4, pp. 1711–1727, 2013, doi: 10.1109/TPEL.2012.2210563.
- [51] R. W. A. A. De Doncker, D. M. Divan, and M. H. Kheraluwala, "A three-phase soft-switched high power density DC/DC converter for high power applications," in *Conference Record of the 1988 IEEE Industry Applications Society Annual Meeting*, Sep. 1991, vol. 27, no. 1, pp. 796–805, doi: 10.1109/IAS.1988.25153.
- [52] J. E. Ochoa Sosa, R. O. Nunez, G. G. Oggier, and G. O. Garcia, "Open transistors fault-tolerant schemes of three-phase dual active bridge DC-DC converters," *IEEE Latin America Transactions*, vol. 19, no. 3, pp. 385–395, 2021, doi: 10.1109/TLA.2021.9447587.
- [53] J. Walter and R. W. De Doncker, "High-power bi-directional DC/DC converter topology for future automobiles," *EPE Journal (European Power Electronics and Drives Journal)*, vol. 14, no. 2, pp. 28–33, 2004, doi: 10.1080/09398368.2004.11463558.
- [54] H. Krishnaswami and N. Mohan, "Three-port series-resonant DC-DC converter to interface renewable energy sources with bidirectional load and energy storage ports," *IEEE Transactions on Power Electronics*, vol. 24, no. 10, pp. 2289–2297, 2009, doi: 10.1109/TPEL.2009.2022756.
- [55] E. E. Henao-Bravo, C. A. Ramos-Paja, A. J. Saavedra-Montes, D. González-Montoya, and J. Sierra-Pérez, "Design method of dual active bridge converters for photovoltaic systems with high voltage gain," *Energies*, vol. 13, no. 7, 2020, doi: 10.3390/en13071711.
- [56] J. Huang, Z. Li, L. Shi, Y. Wang, and J. Zhu, "Optimized modulation and dynamic control of a three-phase dual active bridge converter with variable duty cycles," *IEEE Transactions on Power Electronics*, vol. 34, no. 3, pp. 2856–2873, 2019, doi: 10.1109/TPEL.2018.2842021.
- [57] J.-H. Jung, H.-S. Kim, M.-H. Ryu, and J.-W. Baek, "Design methodology of bidirectional CLLC resonant converter for high-frequency isolation of dc distribution systems," *IEEE Transactions on Power Electronics*, vol. 28, no. 4, pp. 1741–1755, Apr. 2013, doi: 10.1109/TPEL.2012.2213346.
- [58] W. Chen, P. Rong, and Z. Lu, "Snubberless bidirectional DC-DC converter with new CLLC resonant tank featuring minimized switching loss," *IEEE Transactions on Industrial Electronics*, vol. 57, no. 9, pp. 3075–3086, 2010, doi: 10.1109/TIE.2009.2037099.
- [59] H. Chen and A. K. S. Bhat, "A bidirectional dual-bridge LCL-type series resonant converter controlled with modified gating scheme," *2016 IEEE 8th International Power Electronics and Motion Control Conference, IPEMC-ECCE Asia 2016*, pp. 3036–3042, 2016, doi: 10.1109/PEMC.2016.7512780.
- [60] I. W. Hofsjager, J. A. Ferreira, and J. D. van Wyk, "A new manufacturing and packaging technology for the integration of power electronics," in *IAS '95. Conference Record of the 1995 IEEE Industry Applications Conference Thirtieth IAS Annual Meeting*, 1995, vol. 1, pp. 891–897, doi: 10.1109/IAS.1995.530392.
- [61] A. Isurin and A. Cook, "A novel resonant converter topology and its application," *PESC Record - IEEE Annual Power Electronics Specialists Conference*, vol. 2, pp. 1039–1044, 2001, doi: 10.1109/PESC.2001.954256.
- [62] W. L. Malan, D. M. Vilathgamuwa, and G. R. Walker, "Modeling and control of a resonant dual active bridge with a tuned CLLC network," *IEEE Transactions on Power Electronics*, vol. 31, no. 10, pp. 7297–7310, 2016, doi: 10.1109/TPEL.2015.2507787.
- [63] F. C. Lee, S. Wang, P. Kong, C. Wang, and D. Fu, "Power architecture design with improved system efficiency, EMI and power density," in *PESC Record - IEEE Annual Power Electronics Specialists Conference*, Jun. 2008, pp. 4131–4137, doi: 10.1109/PESC.2008.4592602.
- [64] B. Yang and F. C. Lee, "LLC resonant converter for front end DC / DC conversion alpha J. Zhang and Guisong Huang," vol. 00, no. c, pp. 1108–1112, 2002.
- [65] M. Yaqoob, K. H. Loo, and Y. M. Lai, "Modeling the effect of dead-time on the soft-switching characteristic of variable-frequency modulated series-resonant DAB converter," *2017 IEEE 18th Workshop on Control and Modeling for Power Electronics, COMPEL 2017*, 2017, doi: 10.1109/COMPEL.2017.8013306.

- [66] C. Mi, H. Bai, C. Wang, and S. Gargies, "Operation, design and control of dual H-bridge-based isolated bidirectional DC-DC converter," *IET Power Electronics*, vol. 1, no. 4, pp. 507–5017, 2008, doi: 10.1049/iet-pel:20080004.
- [67] P. Xuewei and A. K. Rathore, "Comparison of bi-directional voltage-fed and current-fed dual active bridge isolated dc/dc converters low voltage high current applications," *IEEE International Symposium on Industrial Electronics*, pp. 2566–2571, 2014, doi: 10.1109/ISIE.2014.6865024.
- [68] P. Xuewei and A. K. Rathore, "Novel bidirectional snubberless naturally commutated soft-switching current-fed full-bridge isolated DC/DC converter for fuel cell vehicles," *IEEE Transactions on Industrial Electronics*, vol. 61, no. 5, pp. 2307–2315, 2014, doi: 10.1109/TIE.2013.2271599.
- [69] Z. Ding, C. Yang, Z. Zhang, C. Wang, and S. Xie, "A novel soft-switching multiport bidirectional dc-dc converter for hybrid energy storage system," *IEEE Transactions on Power Electronics*, vol. 29, no. 4, pp. 1595–1609, 2014, doi: 10.1109/TPEL.2013.2264596.
- [70] Z. Guo, K. Sun, T.-F. Wu, and C. Li, "An improved modulation scheme of current-fed bidirectional DC–DC converters for loss reduction," *IEEE Transactions on Power Electronics*, vol. 33, no. 5, pp. 4441–4457, May 2018, doi: 10.1109/TPEL.2017.2719722.
- [71] P. Xuewei and A. K. Rathore, "Novel interleaved bidirectional snubberless soft-switching current-fed full-bridge voltage doubler for fuel-cell vehicles," *IEEE Transactions on Power Electronics*, vol. 28, no. 12, pp. 5535–5546, 2013, doi: 10.1109/TPEL.2013.2252199.
- [72] J. Riedel, D. G. Holmes, B. P. McGrath, and C. Teixeira, "Maintaining Continuous ZVS Operation of a Dual Active Bridge by Reduced Coupling Transformers," *IEEE Transactions on Industrial Electronics*, vol. 65, no. 12, pp. 9438–9448, 2018, doi: 10.1109/TIE.2018.2815993.
- [73] Y. Li, Y. Xing, Y. Lu, H. Wu, and P. Xu, "Performance analysis of a current-fed bidirectional LLC resonant converter," *IECON Proceedings (Industrial Electronics Conference)*, pp. 2486–2491, 2016, doi: 10.1109/IECON.2016.7793163.
- [74] Z. Shen, R. Burgos, D. Boroyevich, and F. Wang, "Soft-switching capability analysis of a dual active bridge dc-dc converter," *IEEE Electric Ship Technologies Symposium, ESTS 2009*, pp. 334–339, 2009, doi: 10.1109/ESTS.2009.4906533.
- [75] E. T. H. Zurich and F. Krismer, "Modeling and optimization of bidirectional dual active bridge DC – DC converter topologies," no. 19177, 2010, doi: 10.3929/ethz-a-006395373.
- [76] A. K. Jain and R. Ayyanar, "PWM control of dual active bridge: Comprehensive analysis and experimental verification," *IEEE Transactions on Power Electronics*, vol. 26, no. 4, pp. 1215–1227, 2011, doi: 10.1109/TPEL.2010.2070519.
- [77] D. Sha, Y. Xu, J. Zhang, and Y. Yan, "Current-fed hybrid dual active bridge DC–DC converter for a fuel cell power conditioning system with reduced input current ripple," *IEEE Transactions on Industrial Electronics*, vol. 64, no. 8, pp. 6628–6638, Aug. 2017, doi: 10.1109/TIE.2017.2698376.
- [78] H. Wu, S. Ding, K. Sun, L. Zhang, Y. Li, and Y. Xing, "Bidirectional soft-switching series-resonant converter with simple PWM control and load-independent voltage-gain characteristics for energy storage system in DC microgrids," *IEEE Journal of Emerging and Selected Topics in Power Electronics*, vol. 5, no. 3, pp. 995–1007, 2017, doi: 10.1109/JESTPE.2017.2651049.
- [79] A. K. Rathore and U. R. Prasanna, "Analysis, design, and experimental results of novel snubberless bidirectional naturally clamped ZCS/ZVS current-fed half-bridge DC/DC converter for fuel cell vehicles," *IEEE Transactions on Industrial Electronics*, vol. 60, no. 10, pp. 4482–4491, 2013, doi: 10.1109/TIE.2012.2213563.
- [80] D. Liu and H. Li, "A ZVS bi-directional DC-DC converter for multiple energy storage elements," *IEEE Transactions on Power Electronics*, vol. 21, no. 5, pp. 1513–1517, 2006, doi: 10.1109/TPEL.2006.882450.
- [81] Z. Wang and H. Li, "A soft switching three-phase current-fed bidirectional DC-DC converter with high efficiency over a wide input voltage range," *IEEE Transactions on Power Electronics*, vol. 27, no. 2, pp. 669–684, 2012, doi: 10.1109/TPEL.2011.2160284.
- [82] H. Pinheiro and P. K. Jain, "Series-parallel resonant UPS with capacitive output DC bus filter for powering HFC networks," *IEEE Transactions on Power Electronics*, vol. 17, no. 6, pp. 971–979, Nov. 2002, doi: 10.1109/TPEL.2002.805595.
- [83] M. H. Kheraluwala, R. W. Gascoigne, D. M. Divan, and E. D. Baumann, "Performance characterization of a high-power dual active bridge dc-to-dc converter," *IEEE Transactions on Industry Applications*, vol. 28, no. 6, pp. 1294–1301, 1992, doi: 10.1109/28.175280.
- [84] M. Nowak, J. Hildebrandt, and P. Luniewski, "Converters with AC transformer intermediate link suitable as interfaces for supercapacitor energy storage," *PESC Record - IEEE Annual Power Electronics Specialists Conference*, vol. 5, pp. 4067–4073, 2004, doi: 10.1109/PESC.2004.1355196.
- [85] R. W. A. De Doncker, D. M. Divan, and M. H. Kheraluwala, "A three-phase soft-switched high-power-density DC/DC converter for high-power applications," *IEEE Transactions on Industry Applications*, vol. 27, no. 1, pp. 63–73, 1991, doi: 10.1109/28.67533.
- [86] O. García, L. A. Flores, J. A. Oliver, J. A. Cobos, and J. De La Peña, "Bi-directional dc-dc converter for hybrid vehicles," *PESC Record - IEEE Annual Power Electronics Specialists Conference*, vol. 2005, pp. 1881–1886, 2005, doi: 10.1109/PESC.2005.1581888.
- [87] A. A. Aboulmaga and A. Emadi, "Performance evaluation of the isolated bidirectional cuk converter with integrated magnetics," *PESC Record - IEEE Annual Power Electronics Specialists Conference*, vol. 2, pp. 1557–1562, 2004, doi: 10.1109/PESC.2004.1355657.
- [88] D. Murthy-Bellur and M. K. Kazimierzczuk, "Isolated two-transistor zeta converter with reduced transistor voltage stress," *IEEE Transactions on Circuits and Systems II: Express Briefs*, vol. 58, no. 1, pp. 41–45, 2011, doi: 10.1109/TCSII.2010.2092829.
- [89] E. V. De Souza and I. Barbi, "Bidirectional current-fed fly back-push-pull DC-DC converter," pp. 8–13, 2011.
- [90] F. D. Esteban, F. M. Serra, and C. H. De Angelo, "Control of a DC-DC dual active bridge converter in DC microgrids applications," *IEEE Latin America Transactions*, vol. 19, no. 8, pp. 1261–1269, 2021, doi: 10.1109/TLA.2021.9475856.
- [91] H. Bai and C. Mi, "Eliminate reactive power and increase system efficiency of isolated bidirectional dual-active-bridge dc-dc converters using novel dual-phase-shift control," *IEEE Transactions on Power Electronics*, vol. 23, no. 6, pp. 2905–2914, 2008, doi: 10.1109/TPEL.2008.2005103.
- [92] B. Zhao, Q. Yu, and W. Sun, "Extended-phase-shift control of isolated bidirectional DC-DC converter for power distribution in microgrid," *IEEE Transactions on Power Electronics*, vol. 27, no. 11, pp. 4667–4680, 2012, doi: 10.1109/TPEL.2011.2180928.
- [93] B. Zhao, Q. Song, and W. Liu, "Power characterization of isolated bidirectional dual-active-bridge dc-dc converter with dual-phase-shift control," *IEEE Transactions on Power Electronics*, vol. 27, no. 9, pp. 4172–4176, 2012, doi: 10.1109/TPEL.2012.2189586.
- [94] B. Zhao, Q. Song, W. Liu, and W. Sun, "Current-stress-optimized switching strategy of isolated bidirectional DC-DC converter with dual-phase-shift control," *IEEE Transactions on Industrial Electronics*, vol. 60, no. 10, pp. 4458–4467, 2013, doi: 10.1109/TIE.2012.2210374.
- [95] K. Rajapandian, V. Ramanarayanan, and R. Ramakumar, "A 250 kHz/560 W phase modulated converter," in *Proceedings of International Conference on Power Electronics, Drives and Energy Systems for Industrial Growth*, vol. 1, pp. 20–26, doi: 10.1109/PEDES.1996.537276.
- [96] F. Krismer and J. W. Kolar, "Accurate small-signal model for the digital control of an automotive bidirectional dual active bridge," *IEEE Transactions on Power Electronics*, vol. 24, no. 12, pp. 2756–2768, 2009, doi: 10.1109/TPEL.2009.2027904.
- [97] A. Tong, L. Hang, G. Li, X. Jiang, and S. Gao, "Modeling and analysis of a dual-active-bridge-isolated bidirectional DC/DC converter to minimize RMS current with whole operating range," *IEEE Transactions on Power Electronics*, vol. 33, no. 6, pp. 5302–5316, 2018, doi: 10.1109/TPEL.2017.2692276.





- [98] F. Krismer and J. W. Kolar, "Closed form solution for minimum conduction loss modulation of DAB converters," *IEEE Transactions on Power Electronics*, vol. 27, no. 1, pp. 174–188, 2012, doi: 10.1109/TPEL.2011.2157976.
- [99] C. Wang and Q. Song, "The research on the triple phase shift control of the isolated bidirectional DC-DC converter," *Proceedings of 2019 IEEE 3rd International Electrical and Energy Conference, CIEEC 2019*, 2019, doi: 10.1109/CIEEC47146.2019.CIEEC-201985.
- [100] D. Mou, Q. Luo, J. Li, Y. Wei, and P. Sun, "Five-degree-of-freedom modulation scheme for dual active bridge DC-DC converter," *IEEE Transactions on Power Electronics*, vol. 36, no. 9, pp. 10584–10601, 2021, doi: 10.1109/TPEL.2021.3056800.
- [101] X. Chen, G. Xu, H. Han, D. Liu, Y. Sun, and M. Su, "Light-Load Efficiency Enhancement of High-frequency Dual-Active-Bridge Converter under SPS Control," *IEEE Transactions on Industrial Electronics*, vol. 68, no. 12, pp. 12941–12946, 2021, doi: 10.1109/TIE.2020.3044803.
- [102] J. Guacaneme, G. Garcerá, E. Figueres, I. Patrao, and R. González-Medina, "Dynamic modeling of a dual active bridge DC to DC converter with average current control and load-current feed-forward," *International Journal of Circuit Theory and Applications*, vol. 43, no. 10, pp. 1311–1332, 2015, doi: 10.1002/cta.2012.
- [103] X. Pan, H. Li, Y. Liu, T. Zhao, C. Ju, and A. K. Rathore, "An Overview and comprehensive comparative evaluation of current-fed-isolated-bidirectional DC/DC converter," *IEEE Transactions on Power Electronics*, vol. 35, no. 3, pp. 2737–2763, 2020, doi: 10.1109/TPEL.2019.2931739.
- [104] G. J. Su and L. Tang, "A multiphase, modular, bidirectional, triple-voltage dc-dc converter for hybrid and fuel cell vehicle power systems," *IEEE Transactions on Power Electronics*, vol. 23, no. 6, pp. 3035–3046, 2008, doi: 10.1109/TPEL.2008.2005386.
- [105] R. Lenke, F. Mura, and R. W. De Doncker, "Comparison of non-resonant and super-resonant dual-active ZVS-operated high-power DC-DC converters," *2009 13th European Conference on Power Electronics and Applications, EPE '09*, 2009.
- [106] K. Wang, C. Y. Lin, L. Zhu, D. Qu, F. C. Lee, and J. S. Lai, "Bi-directional dc to dc converters for fuel cell systems," *IEEE Workshop on Power Electronics in Transportation*, pp. 47–51, 1998, doi: 10.1109/pet.1998.731056.
- [107] X. Sun, X. Wu, Y. Shen, X. Li, and Z. Lu, "A Current-Fed Isolated Bidirectional DC-DC Converter," *IEEE Transactions on Power Electronics*, vol. 32, no. 9, pp. 6882–6895, 2017, doi: 10.1109/TPEL.2016.2623306.

BIOGRAPHIES OF AUTHORS







Kiran Bathala     (Student Member, IEEE) received a Bachelor's Degree in Electrical and Electronics Engineering from Jawaharlal Nehru Technological University Anantapur (SVCET), India, in 2009. He completed his Master's Degree from National Institute of Technology Calicut, India, in 2012. Currently continuing his Ph.D. degree in Electrical & Electronics Engineering in National Institute of Technology, Karnataka, India from 2017. Before joining his Ph.D., he was working as Asst. Professor in SVCET Chittoor, A.P, India from 2012-2016. His research interests are Power electronics in integrating renewable energy resources with energy storage systems. Soft switching Converters. He can be contacted at email: kiran0219@gmail.com.



Dharavath Kishan     (Senior Member, IEEE) received a Bachelor Degree in Electrical and Electronics Engineering from Jawaharlal Nehru Technological University, Hyderabad (MRET), 2011. He completed his Master's Degree from degree in Electrical & Electronics Engineering from Jawaharlal Nehru Technological University, Hyderabad (CMRCET), India, in 2013. He received his Ph.D., Degree from National Institute of Technology Tiruchirapalli, India, in 2018. Currently serving as Assistant Professor with Department of Electrical & Electronics Engineering, National Institute of Technology Karnataka, India. His research interests are Wireless Battery Charging, Smart transportation and electrification and Electric energy storage systems and motor drives for Transportation Electrification. He can be contacted at email: kishand@nitk.edu.in.



Nagendrappa Harischandruppa     (Senior Member, IEEE) received the B.E. Degree in Electrical and Electronics Engineering and the M.Tech. degree in Power and Energy Systems from the National Institute of Technology Karnataka, India, in 1999 and 2002, respectively, and the Ph.D. degree in electrical engineering from the University of Victoria, Victoria, BC, Canada, in 2015. He is currently working as an Assistant Professor with Department of Electrical & Electronics Engineering, National Institute of Technology Karnataka, India. For a short period, he was an Assistant Engineer (operation and maintenance) with the Power Distribution Utility, Mangalore Electricity Supply Company (MESCOM) Ltd., Ajjampura, India. His research interests include high frequency soft-switching converters for power generation from renewable energy sources and their grid-interfacing applications. He can be contacted at email: nagendrappa@nitk.edu.in.